地質調査研究報告

BULLETIN OF THE GEOLOGICAL SURVEY OF JAPAN

表紙の図

東北日本の東西短縮テクトニクスの原因

　大部分がユーラシアプレートに属する日本列島には，南からフィリピン海プレートが，東から太平洋プレートが沈み込んでいる．これら 3 つのプレートの運動と，3 つの収束境界(海溝)が一点に集まる海溝型三重会合点の三次元幾何学を組み合わせた思考実験を行った．その結果，三重会合点で太平洋プレートが切断されないとする条件のもとでフィリピン海プレートが現在の運動を行うと，東北日本が必然的に西に移動し，島弧近くは東西に短縮せざるを得ないことが判明した．このことは，内陸地震の原因が太平洋プレートの運動そのものではなく，日本海溝(沈み込み位置)を移動させているフィリピン海プレートの運動であることを表している．

(図・文：高橋雅紀)

Cover Figure

The cause of the east-west contraction of Northeast Japan

　Geodynamic flame work of the Japanese Islands. The Philippine Sea Plate motion will cause the Izu–Ogasawara Trench to migrate westward, then T–T–T triple junction, Japan Trench, and NE Japan successively. Thereby, the arc crust of NE Japan has no choice but to shorten its width as it drifts westward. The cause of inland earthquakes along the Japan Sea side of NE Japan is the Philippine Sea Plate, not the Pacific Plate. It is the imposed displacement arising from moving subduction boundary of the Pacific Plate (Japan Trench) that causes the E–W contraction of NE Japan, not the Pacific Plate motion itself.

(Figure and Caption by Masaki Takahashi)

論文 - Article

石川県輪島市（能登半島）に分布する中新統から産出した珪藻化石

柳沢幸夫[1,*]

Abstract: Diatoms of the Miocene Wajima and Tsukada formations distributed in Wajima City (Noto Peninsula, Ishikawa Prefecture) were examined. Non-marine lacustrine diatoms are found in the uppermost part of the Wajima Formation. The Tsukada Formation contains middle Miocene diatom assemblages which can be placed between the biohorizons D53 (12.3 Ma) and D54 (11.6 Ma) of the *Denticulopsis praedimorpha* Zone (NPD5B). An unconformity at the base of the Tsukada Formation ranging from ca. 16 Ma to 12.3 Ma indicates that a land area might be present in the western part of Noto Peninsula during the early Middle Miocene.

Keywords: diatom, biostratigraphy, marine, diatomite, Miocene, Tsukada Formation, Wajima, Noto, Ishikawa Prefecture, Japan

要 旨

石川県輪島市（能登半島）の市街地周辺に分布する中新統の輪島層と塚田層の珪藻化石分析を行い，層序・年代及び古地理に関する新たな知見が得られた．輪島層からは湖沼生の珪藻化石が産出し，輪島層の一部に湖沼成堆積物が存在することが明らかとなった．塚田層からはNPD5B帯上部に属する海生珪藻化石が産出し，本層の年代が 12.3–11.6 Ma であることが判明した．塚田層の基底には明瞭な不整合が存在し，輪島層と塚田層の堆積期の間，輪島市の内陸を含む能登半島西部には陸域が存在していたと推定される．

1．はじめに

石川県輪島市（第1図）で生産される輪島塗は，その優美さとともに，長期間の使用に耐えうる堅牢性でよく知られている．この堅牢性の秘密は，輪島市街の通称小峰山（こみねやま）から産出する珪藻土を数百℃で焼成し粉砕・篩い分けして作られる「地の粉（ぢのこ）」と呼ばれる粉末を生漆・米糊と混ぜて下地を厚く何層も塗ることにある．

「地の粉」の原料となる珪藻土は中新統の塚田層に属し，含有される珪藻化石については，すでに市川・絈野（1963）や奥野（1973）によって詳しく研究されている．また，塚田層の地質年代については，小林ほか（2005）が報告している 1 試料の珪藻年代データと，柳沢（2012）が「地の粉」の原料の試料を分析した珪藻データがある．しかし，塚田層全体の年代範囲は曖昧なままであった．

2013 年 11 月 17 日と 18 日の両日，輪島市において，漆サミット 2013 in 輪島（主催：漆サミット in 輪島実行委員会・漆サミット実行委員会）が開催され，漆や漆芸に関するさまざまな研究発表が行われた．著者はこのシンポジウムの招待講演者として「地の粉」の原料となる珪藻土に関する講演を行った（柳沢，2013）．シンポジウム終了後，若干の時間があり，塚田層とその下位の輪島層について地質調査と珪藻試料の採取を行う機会を得た．調査時間が無く十分な調査はできなかったため，層序や地層分布については疑問が残ったままであるが，採取した試料の分析結果は輪島地域の地質に関する今後の研究において重要と判断されるので，ここに簡単に報告する．

2．地質概説

輪島市市街地付近に分布する中新統は，絈野（1965, 1993），Fuji (1972) 及び小林ほか（2005）によって調査・研究がなされている．ここでは能登半島全域を総括している絈野（1965, 1993）の層序を暫定的に使用する．ただし，これらの報告では，地層区分や地層名が異なるだけでなく，地層分布にも大きな食い違いがあり，輪島地域の新第三系については岩相層序の基本的な枠組みを含めた再検討が必要であろう．

絈野（1965）によれば，輪島市付近の中新統は，下位

---

[1] 産業技術総合研究所 地質調査総合センター 地質情報研究部門 (AIST, Geological Survey of Japan, Research Institute of Geology and Geoinformation)

*Corresponding author: Y. Yanagisawa, Central 7, Higashi 1-1-1, Tsukuba, Ibaraki 305-8567, Japan, Email: y.yanagisawa@aist.go.jp
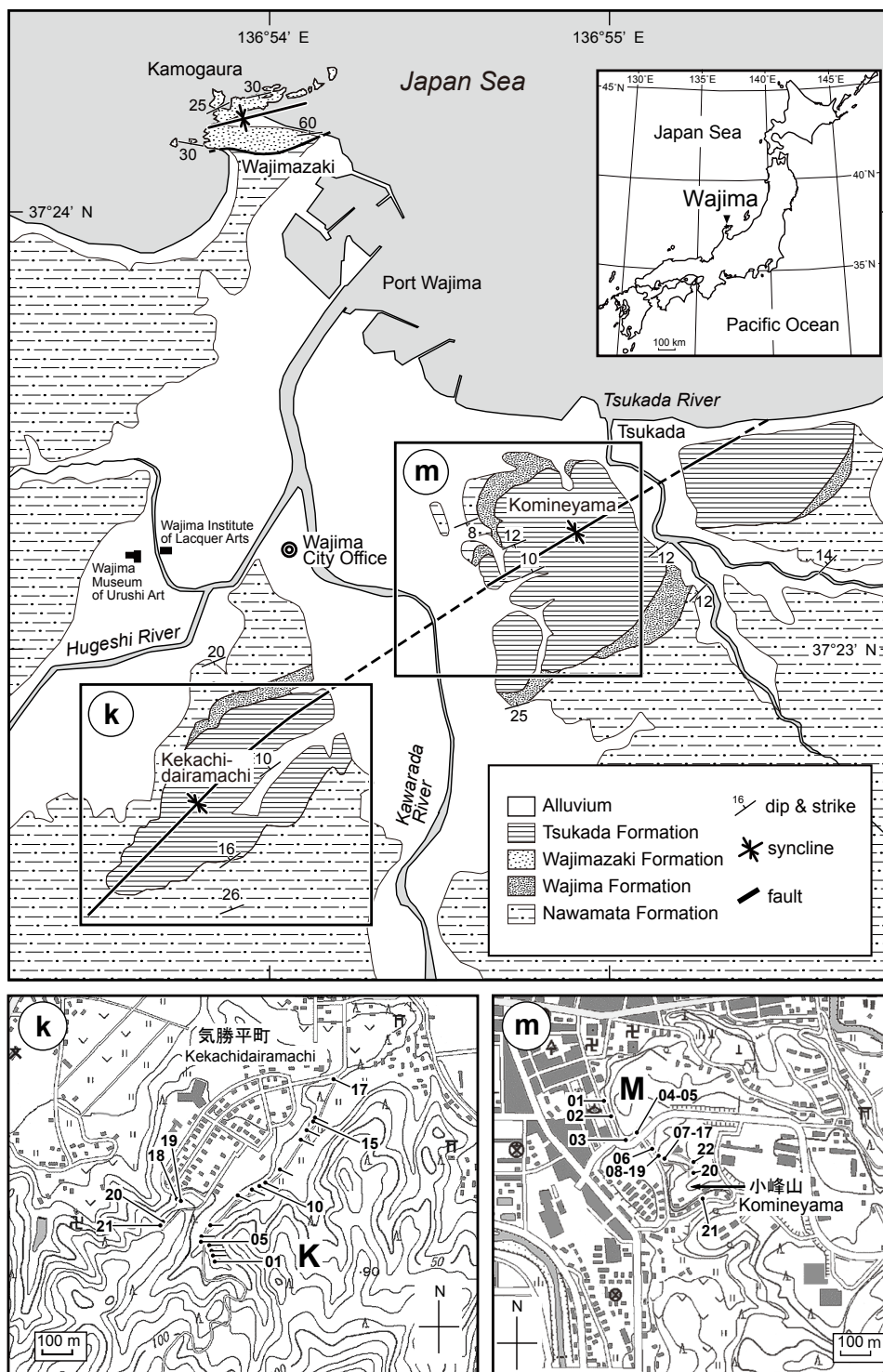
第1図　輪島地域の地質図と試料採取位置図．地質図はFuji（1972），絀野（1993），小林ほか（2005）を基に本研究の
　　　　調査結果を加えて編纂．気勝平町（k：K01–K21）と小峰山（m：M01–21）における試料採取位置図は国土地理院発
　　　　行2万5千分の1地形図「輪島」を使用．試料採取位置図におけるKとMは試料番号の頭文字を示す．

Fig. 1　Geologic map of the Wajima area, Ishikawa Prefecture, Japan based on Fuji (1972), Kaseno (1993), Kobayashi *et al*. (2005)
　　　　and this study, with location maps of samples. Geographical map of "Wajima" (1: 25,000 in scale) of Geospatial Information
　　　　Authority of Japan is used. Characters K and M in sample location maps indicate the initials of sample numbers.

より縄又層，輪島層及び塚田層からなる（第1図）．なお，絎野（1965）では，これらの地層をそれぞれ「縄又層」または「縄又互層」，「輪島互層」及び「塚田泥岩層」と呼んでいるが，ここでは日本地質学会の地層命名の指針に従って，縄又層，輪島層及び塚田層という地層名で統一する．また，絎野（1993）及び小林ほか（2005）では，本報告の輪島層を「東印内層」と呼んでいるが，輪島は東印内層の模式地とは遠く離れており，輪島層とした地層が模式地の東印内層に対比できるかどうか確実ではないので，ここでは輪島層の地層名を使用する．

　縄又層は砂岩，泥岩及び礫岩からなる陸成層である．本層の主体は網状河川の堆積物と考えられるが，一部で保存不良の湖沼生珪藻化石が産出することなどから，湖沼成堆積物も含まれていると推定される（小林ほか，2005）．

　輪島層は砂岩・砂質泥岩・礫岩及び凝灰岩からなる．本層からは，*Anadara* sp.，*Batillaria* sp. などのArcid-Potamid群集と思われる貝類化石と，*Pecten* sp.，*Chlamys* sp. などのPectinid群集に相当する貝類化石，それに*Operculina*や*Miogypsina*などの大型海生有孔虫が産出している（絎野，1965）．また，後述するように本調査において本層から淡水湖沼生の珪藻化石群集が産出した．以上の産出化石から，本層は淡水陸成堆積物，Arcid-Potamid群集を産する内湾・潮間帯を含むエスチュアリー堆積物，そしてPectinid群集や大型有孔虫化石を産する外洋性浅海成堆積物からなることが推察されるが，これら堆積環境の異なる岩相の相互の関係は現状では不明である．輪島層と下位の縄又層との層序関係は不整合と推定されているが（絎野，1965），その根拠は確かではない．塚田層は無層理の珪藻質泥岩からなる海成層である．下位の輪島層とは不整合関係にあると考えられてきたが，その証拠は示されていない（絎野，1965, 1993）．

　このほか，本調査範囲からははずれるが，輪島港北西の輪島崎町鴨ヶ浦付近には，輪島崎層が分布する（第1図；絎野，1965）．小林ほか（2005）は輪島崎層と縄又層の関係を不整合としているが，絎野（1965, 1993）及び上ほか（1981）は輪島崎層と縄又層は断層で接するとしている．本層の主体は石灰質砂岩からなり，各種貝類化石のほか，ウニの破片，こけ虫，有孔虫及び石灰質ナノ化石を産する．本層の最上部約5 mは細粒の海緑石砂岩からなる．

3．試料・方法

　珪藻化石試料の採取は，「地の粉」を採掘している輪島漆器商工業組合の地の粉工場がある小峰山周辺（第1図m）と，河原田川を挟んで対岸にあたる気勝平町周辺（けかちだいらまち）（第1図k）で行った．小峰山ルートではM01–M22の22個，気勝平町ルートではK01–K21の21個の試料を採取した．

　試料の処理は，Akiba（1986）のunprocessed strewn slide

の作成方法で行った．乾燥試料は新聞紙でくるみ，ハンマーで砕いた後，約1gを100 mlビーカーに入れ，試料が浸る程度に純水を注ぎ入れ，一昼夜放置する．この過程で試料はほとんど泥化する．次にビーカーに純水を加えて約100 mlの懸濁液とし，約20秒間放置して粗粒物が底に沈むのを待ち，上澄みの懸濁液からマイクロピペットで0.5 mlを取り出し，18 x 18 mmのカバーグラスに滴下する．これをホットプレートで加熱・乾燥後，アルコールで薄めたPleurax（封入剤）をカバーグラスに滴下し，さらに加熱・乾燥させてアルコール分を蒸発させる．最後に，このカバーグラスをホットプレートで温めたスライドグラスに貼付する．

　珪藻殻の計数は，生物顕微鏡600倍の倍率下で，*Chaetoceros*属の休眠胞子を除いて，観察されたすべての種の蓋殻が50になるまで行った．その後，さらにカバーグラスの幅5 mmの範囲を走査して，その過程で新たに認められた種，及び破片としてのみ認められた種はpresent（＋）として記録した．休眠胞子については，上記蓋殻計数時に認められた総数を別途記録した．

　珪藻化石帯区分はAkiba（1986）とYanagisawa and Akiba（1998）の新第三紀北太平洋珪藻化石帯区分を適用し，化石帯はNPDコード，生層準はDコード（D10–D120）を用いた．珪藻年代はWatanabe and Yanagisawa（2005）を用いて修正し，Gradstein *et al.*（2012）の地磁気極性年代尺度に合わせて調整した．なお，記載を簡便にするため，ここでは珪藻化石帯のNPD5B帯を，生層準を基準にして暫定的に5B1, 5B2, 5B3, 5B4の4区間に分けた．

4．結　果

4．1　小峰山ルート

　このルートは，下位より縄又層，輪島層及び塚田層からなり，全体の層厚は約60 mである（第2図m）．小峰山ルートの縄又層は，層厚約20 mで，青灰色塊状泥岩，斜交層理の発達した中〜粗粒砂岩の繰り返しを主とし，小礫からなる礫岩層が挟まる．このルートの輪島層は，層厚は最大4 m程度で塊状ないし不明瞭な葉理のある青灰色泥岩からなる．下位の縄又層との層序関係は露出不良で確認できない．塚田層は塊状の珪藻質泥岩からなる．基底には厚さ30 cmの中礫岩層があり，下位の輪島層の泥岩を不整合に覆うのが観察できる．その上位には厚さ5 cmほどの礫岩層を挟み，一部軽石片が散在する珪藻質泥岩（厚さ70 cm）があり，さらにその上に硬質泥岩（厚さ60 cm）が重なる．その上位は塊状の珪藻質泥岩からなるが，基底から約6 mの層準には葉理のある白色ガラス質珪長質火山灰層（層厚5 cm）が挟在する．採取した22試料のうち，縄又層の泥岩試料（M01–05）からは珪藻化石は産出しなかった．輪島層の試料M06–10では，M10からは珪藻が検出されなかったが，残り
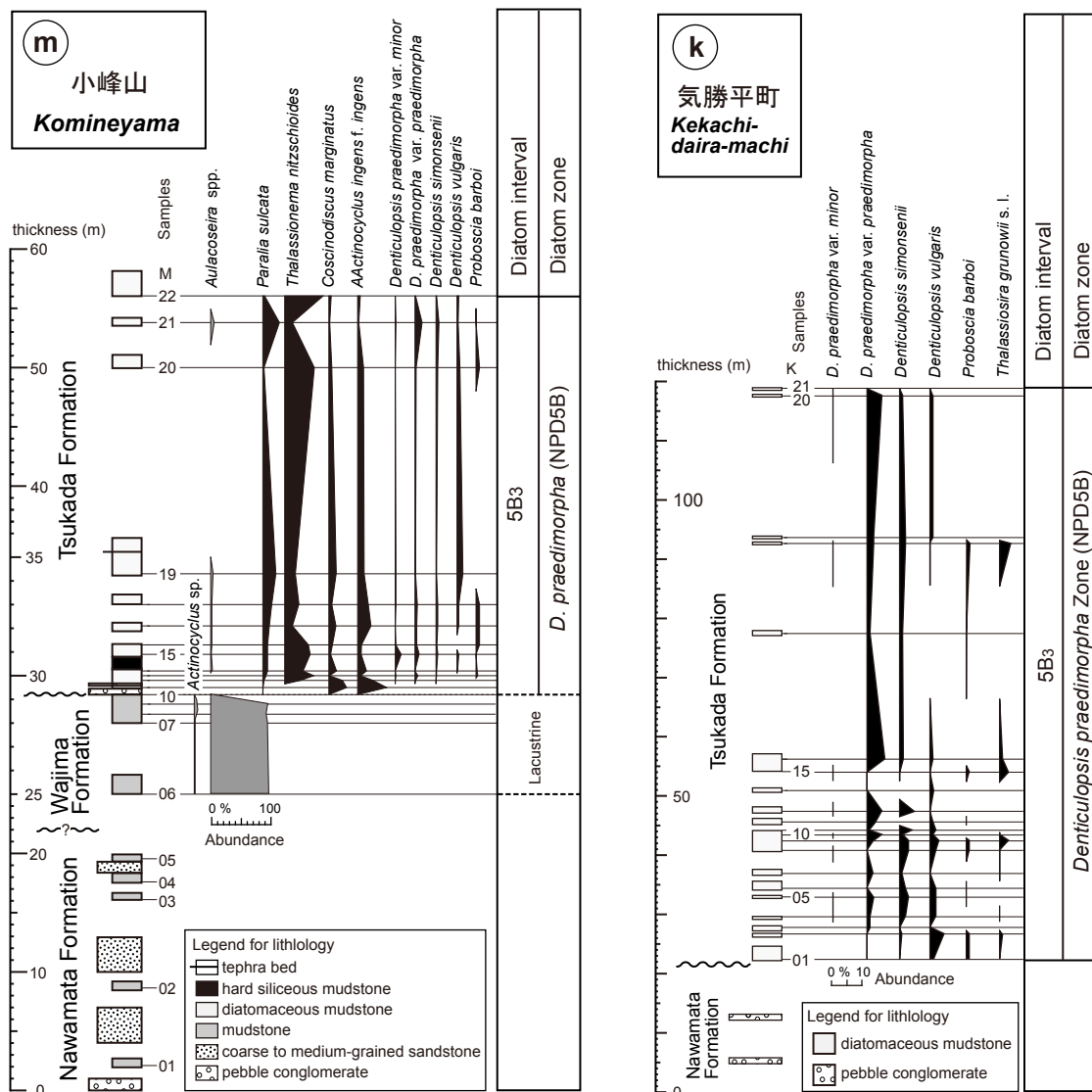
第2図　輪島市小峰山ルート（m）及び気勝平町ルート（k）での主な珪藻種の層序的分布．小峰山ルートにおける層厚の
　　　　スケールは，25–36 m の区間のみ 2 倍に拡大している．

Fig. 2　Stratigraphic distribution of selected diatom species in Komineyama (m) and Kekachidairamachi (k) routes, Wajima
　　　　City. Scale bar of thickness between 25 m and 36 m in the Komineyama route is exaggerated twice.

の試料からは珪藻化石が産出した（第1表）．浮遊性の
Aulacoseira spp.（94–98%）と *Actinocyclus* sp.（2–6%）が優
占し，これに 1% 以下の底生種 *Tetracyclus* sp. *Epithemia*
sp. 及び *Eunotia* sp. などを伴う．いずれの種も淡水生であ
り，浮遊性種が優占することから，このルートの輪島層
の泥岩は湖沼で堆積したものと推定される．

　塚田層の試料 M11–22 からは海生の珪藻化石が産出し
た．ただし，最下位の M11 は珪藻の含有量が小さく，プ
レパラート全面を走査しても珪藻蓋殻は 20 個に留ま
り，珪藻化石帯の認定はできなかった．残りの M12–22
からは珪藻化石が豊富に産出した（第1表）．産出した

主な珪藻は，*Actinocyclus ingens* f. *ingens*，*Coscinodiscus
marginatus*，*Denticulopsis praedimorpha* var. *minor*，*D.
praedimorpha* var. *praedimorpha*，*D. simonsenii*，*D.
vulgaris*，*Paralia sulcata*，*Proboscia barboi*，*Thalassionema
nitzschioides* などである．これらの種のうち，珪藻化
石層序の年代指標となるのは，*D. praedimorpha* var.
praedimorpha である．このタクソンは生層準 D53（*D.
praedimorpha* var. *praedimorpha* の初産出層準）で出現し，
D55（*D. praedimorpha* の終産出層準）で絶滅する．また，
このルートでは生層準 D54（*D. praedimorpha* var. *robusta*
の初産出層準）で出現する *D. praedimorpha* var. *robusta* は

第1表　輪島市小峰山ルートの珪藻化石産出表.

Table 1　Occurrence chart of diatoms in the Komineyama route, Wajima City.

	Wajima F.				Tsukada Formation											
Formation	lacustrine				*Denticulopsis praedimorpha* Zone (NPD5B)											
Diatom zones																
Sample number (M)	06	07	08	09	11	12	13	14	15	16	17	18	19	20	21	22
Original sample number (Noto)	1368	1377	1376	1375	1373	1372	1371	1370	1379	1378	1380	1369	1367	1386	1366	1365
Preservation	P	P	M	M	P	P	P	P	M	P	P	P	P	M	M	M
Abundance	A	A	A	A	R	R	C	R	R	R	C	R	C	C	C	C
Marine diatoms																
Actinocyclus ellipticus Grunow	-	-	-	-	-	-	-	2	-	-	-	-	-	-	-	-
A. ingens f. *ingens* (Rattray) Whiting et Schrader	-	-	-	-	10	26	5	15	6	7	22	18	11	10	2	4
A. octonarius Ehr.	-	-	-	-	-	5	1	1	2	7	6	7	-	-	1	-
A. sp. A	-	-	-	-	-	-	-	-	-	-	-	-	-	-	-	3
Actinoptychus senarius (Ehr.) Ehr.	-	-	-	-	-	2	2	1	1	2	5	1	2	3	3	2
Arachnoidiscus spp.	-	-	-	-	-	-	1	-	-	-	-	-	-	-	-	-
Azpeitia endoi (Kanaya) P.A.Sims et G.A.Fryxell	-	-	-	-	-	1	-	-	1	-	-	-	-	-	-	-
A. vetustissima (Pant.) P.A.Sims	-	-	-	-	-	-	3	1	-	-	2	-	1	-	-	-
*Cavitatus jouseanus (*Sheshukova*)* D.M.Williams	-	-	-	-	-	-	-	2	-	+	-	+	-	-	-	-
C. miocenicus (Schrader*)* Akiba et Yanagisawa	-	-	-	-	-	+	+	-	1	-	-	-	+	-	+	-
Cocconeis californica Grunow	-	-	-	-	-	-	-	-	-	-	1	-	-	-	-	-
C. curviritunda Brun et Temp.	-	-	-	-	-	-	-	-	-	-	-	-	-	-	1	-
C. scutellum Ehr.	-	-	-	-	-	-	-	-	-	-	-	-	-	-	2	-
C. vitrea Brun	-	-	-	-	-	-	-	-	-	-	-	-	-	-	1	1
Coscinodiscus marginatus Ehr.	-	-	-	-	6	23	1	13	3	6	12	5	13	5	2	4
C. radiatus Ehr.	-	-	-	-	-	-	-	-	-	-	-	-	-	-	-	1
C. spp.	-	-	-	-	-	-	5	7	-	1	-	-	-	-	2	-
Delphineis biseriata (Grunow) G.W.Andrews	-	-	-	-	-	-	-	-	-	1	-	-	-	-	-	-
Denticulopsis praedimorpha var. *minor* Yanagisawa et Akiba	-	-	-	-	-	+	1	-	10	1	-	1	1	-	1	+
(Closed copula)	-	-	-	-	-	-	2	4	6	3	1	3	3	2	1	2
D. praedimorpha var. *praedimorpha* Barron ex Akiba	-	-	-	-	-	1	5	+	7	3	3	4	1	2	12	1
(Closed copula)	-	-	-	-	-	+	5	3	7	2	8	5	1	2	15	13
D. simonsenii Yanagisawa et Akiba	-	-	-	-	-	+	1	1	3	2	3	3	1	3	5	1
D. vulgaris (Okuno) Yanagisawa et Akiba	-	-	-	-	-	-	2	1	+	3	3	3	-	3	+	-
S-type girdle view of *D. simonsenii* group	-	-	-	-	-	+	1	1	-	2	6	4	+	4	2	1
Diploneis bombus Ehr.	-	-	-	-	-	-	+	-	-	-	-	1	-	-	-	-
D. smithii (Bréb.) Cleve	-	-	-	-	-	-	-	3	-	1	1	1	1	1	3	1
Eucampia sp. A	-	-	-	-	-	1	-	-	-	-	-	-	-	-	-	-
Goniothecium rogersii Ehr.	-	-	-	-	-	-	-	-	-	-	-	-	-	-	1	-
Grammatophora spp.	-	-	-	-	+	+	+	+	1	-	+	1	1	-	+	+
Hyalodiscus obsoletus Sheshukova	-	-	-	-	-	1	1	2	1	2	1	2	4	3	5	2
Ikebea tenuis (Brun) Akiba	-	-	-	-	-	+	-	-	-	-	-	-	-	-	-	-
Melosira sol (Ehr.) Kützing	-	-	-	-	-	-	-	1	3	-	-	-	3	-	-	-
Navicula sp.	-	-	-	-	-	-	2	-	-	-	-	-	-	-	-	-
Nitzschia heteropolica Schrader	-	-	-	-	-	-	-	-	+	+	+	1	-	1	+	-
Odontella aurita (Lyngb.) J.A.Agardh	-	-	-	-	-	-	-	-	-	-	-	-	-	-	2	-
Paralia sulcata (Ehr.) Cleve	-	-	-	-	1	2	6	8	8	8	11	15	22	2	28	4
Proboscia barboi (Brun) Jordan et Priddle	-	-	-	-	-	-	-	1	3	-	3	3	10	5	2	3
Rhizosolenia hebetata f. *hiemalis* Gran	-	-	-	-	-	-	-	-	1	-	-	-	-	-	-	-
R. miocenica Schrader	-	-	-	-	-	-	1	-	-	5	-	-	-	-	-	-
R. styliformis Brightw.	-	-	-	-	-	1	3	2	5	1	-	1	-	1	-	2
Stellarima microtrias (Ehr.) Hasle et P.A.Sims	-	-	-	-	-	2	-	-	-	1	-	-	-	-	-	-
Stephanogonia hanzawae Kanaya	-	-	-	-	-	-	-	3	-	-	-	-	-	1	2	-
Stephanopyxis spp.	-	-	-	-	3	6	1	-	-	1	1	1	2	4	-	1
Thalassionema hirosakiensis (Kanaya) Schrader	-	-	-	-	-	-	5	-	-	-	-	-	4	1	5	4
Non-marine diatoms																
T. nitzschioides (Grunow) H. Perag. et Perag.	-	-	-	-	-	27	49	31	43	40	13	24	18	50	13	64
Thalassiosira grunowii Akiba et Yanagisawa	-	-	-	-	-	2	4	1	-	4	2	-	-	1	-	1
T. praenidulus Akiba	-	-	-	-	-	-	-	-	-	-	3	1	-	-	-	-
Thalassiothrix longissima Cleve et Grunow	-	-	-	-	-	-	-	+	-	-	-	-	-	-	-	-
Actinocyclus sp.	2	2	6	4	-	-	-	-	-	-	-	-	-	-	-	-
Aulacoseira spp.	98	96	94	96	-	-	-	3	1	2	2	2	4	-	6	-
Epithemia sp.	-	1	-	-	-	-	-	-	-	-	-	-	-	-	-	-
Eunotia sp.	-	-	-	+	-	-	-	-	-	-	-	-	-	-	-	-
Tetracyclus sp.	+	1	-	-	-	-	-	-	-	-	-	-	-	-	-	-
Total number of valves counted	100	100	100	100	20	100	100	100	100	100	100	100	100	100	100	100
Resting spore of *Chaetoceros*	0	0	0	0	0	37	77	51	24	71	52	43	65	76	92	22
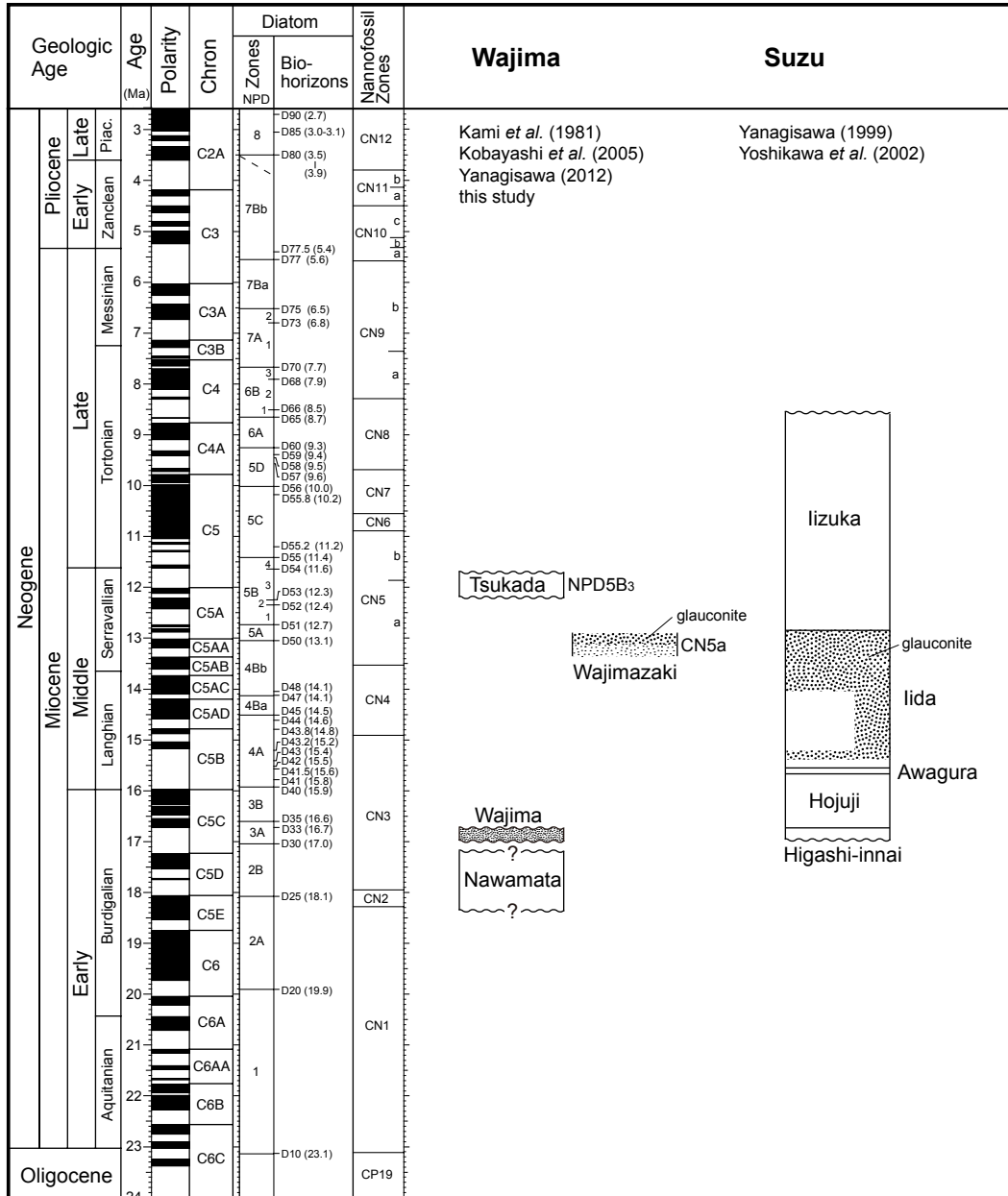
第3図　塚田層の年代と珠洲地域の地層との対比. 珪藻化石層序はAkiba（1986），Yanagisawa and Akiba（1998）及び Watanabe and Yanagisawa（2005）に基づく. 珪藻生層準の年代は Gradstein *et al.*（2012）の地磁気極性年代尺度との対比に基づいて算定.

Fig. 3　Age of the Tsukada Formation and correlation to the Miocene sequence in the Suzu area, Noto Peninsula, Ishikawa Prefecture. Diatom biostratigraphic zonation used in this paper is that proposed by Akiba (1986), and modified by Yanagisawa and Akiba (1998) and Watanabe and Yanagisawa (2005). Ages of marker diatom biohorizons are calibrated by correlation to a geomagnetic time scale of Gradstein *et al.* (2012).

産出しない. 以上のことから，小峰山ルートの塚田層は，*Denticulopsis praedimorpha*帯（NPD5B帯）に属し，さらにその上部の生層準D53（12.3 Ma）とD54（11.6 Ma）の間，すなわち区間 NPD5B3 に位置づけられる（第3図）.

4. 2　気勝平町ルート

試料は気勝平町団地の南東の沢沿いで採取したK01–17と，団地南西端の潮見台公園付近で採取したK18–21である（第1図k）. このルートは縄又層と塚田層からなる. 縄又層は小礫大の円礫ないし亜角礫からなる礫支持

の礫岩である．塚田層は塊状の珪藻質泥岩からなる．

採取したすべての試料から保存のよい海生珪藻化石が産出した（第2表）．ほぼ連続して産出したのは *Denticulopsis praedimorpha* var. *minor*, *D. praedimorpha* var. *praedimorpha*, *D. simonsenii*, *D. vulgaris*, *Proboscia barboi*, *Thalassiosira grunowii* s. l. などである（第2図k）．このうち，珪藻化石層序の年代指標となるのは，*D. praedimorpha* var. *praedimorpha*であり，小峰山ルートと同様に気勝平ルートの塚田層は，*D. praedimorpha*帯（NPD5B帯）の区間 NPD5B3に対比できる．

5．考　察

5．1　塚田層の年代と対比

小峰山ルート及び気勝平ルートにおける塚田層は，どちらも珪藻化石層序区分のNPD5B帯の区間 NPD5B3（12.3–11.6 Ma）に対比できる．また，柳沢（2012）が報告した「地の粉」の原料となった，小峰山で採掘された風化珪藻質泥岩の試料も全く同じ区間に含められる．以上のことから，塚田層の年代は12.3 Maから11.6 Maの間にあると考えられる（第3図）．

ところで，輪島市東方の能登半島北東端にあたる珠洲地域に分布する海成中新統の層序及び珪藻化石層序については非常に詳しい研究が行われ，正確な年代が判明している（柳沢，1999；吉川ほか，2002）．その結果と今回の成果を比較すると，輪島地域の塚田泥岩層の試料は，珠洲地域の飯塚層最下部に対比できる（第3図）．

5．2　輪島地域の中新統の年代層序のまとめ

輪島地域に分布する中新統の年代分布は第3図のようにまとめられる．

縄又層からは広い意味での台島型植物群が産出する（絈野，1965；Fuji, 1972；小林ほか，2005）ため，その年代は前期中新世であると推定されるが，具体的な数値年代を示すデータは得られていない．

輪島層からは，*Anadara* sp.や *Batillaria* sp. などのArcid-Potamid 群集に属する貝類化石と，*Pecten* sp.や *Chlamys* sp. などのPectinid 群集に相当する貝類化石のほか，*Operculina*や *Miogypsina* などの大型海生有孔虫が産出している（絈野，1965）．これらは，広い意味での八尾-門ノ沢動物群に属し，珠洲地域の東印内層と共通する．東印内層の上位の法住寺層の下限は，珪藻化石帯*Crucidenticula kanayae*帯（NPD3A帯）上部の生層準D33（16.7 Ma）付近に位置する（柳沢，1999；吉川ほか，2002）．したがって，東印内層は16.7 Maより古いことは確かであるが，下限の年代は不確かである．ただし，東印内層は層厚が数十m以下と薄く，かつ本層が河川成ないしエスチュアリー堆積物などの堆積速度が速いと思われる堆積物からなることから，その堆積時間は比較的短

いと推定され，吉川ほか（2002）では東印内層の下限年代を約17 Maとしている．東印内層に対比される輪島層も東印内層と同程度の年代である可能性が高い．

塚田層は既述のように*Denticulopsis praedimorpha*帯（NPD5B帯）の区間NPD5B3（12.3–11.6 Ma）に相当するので，その堆積年代はこの年代区間内に収まる．

輪島崎層は，上ほか（1981）によればOkada and Bukry（1980）の石灰質ナノ化石帯区分のCN5a帯に対比できるとされており，年代は13.55–12.85 Maの区間内にあると言える．本層は孤立して分布するため，塚田層との上下関係は不明であるが，輪島崎層の最上部に発達する海緑石砂岩層が，珠洲地域の飯田層最上部の海緑石砂岩層に相当するとみられることから，おそらく塚田層よりは古い堆積物と思われる（第3図）．この対比案は従来の見解（絈野，1965；小林ほか，2005）と同じである．

5．3　塚田層基底の不整合の意義

塚田層は下位の輪島層を不整合に覆うとされてきた（絈野，1965）．小林ほか（2005）も輪島市久手川町で輪島層に属する亜炭層を挟む砂岩礫岩互層を塚田層が直接不整合に覆う露頭を確認している．本研究でも，小峰山ルートにおいて，輪島層の湖沼成泥岩を塚田層が直接覆う露頭が観察された（第2図）．基底に礫岩層を伴い，基底面に凹凸もみられるので，この不整合は陸上浸食によって形成された可能性が高い．このことから，輪島層堆積後から塚田層堆積前の時期（約16–12 Ma）に，輪島地域の内陸部は陸化して浸食を受けていたと推定できる．これに対して，海岸部の輪島崎では，この時期に少なくとも浅海の石灰質砂岩層からなる輪島崎層が堆積していたことから，海陸境界は小峰山と輪島崎の間に存在したものと思われる．一方，輪島東方の珠洲地域では，この時期には連続して海成層が堆積しており（第3図），一貫して海域であったことを示している．したがって，陸域は能登半島の西部にのみ存在していたものと思われる．

6．まとめ

本研究では，石川県輪島市（能登半島）の市街地周辺に分布する中新統の珪藻化石分析を行った．その結果，本地域の中新統の層序と年代及び古地理に関する新たな知見が得られた．

(1) 縄又層からは珪藻化石は産出しなかったが，輪島層からは*Aulacoseira* spp.及び*Actinocyclus* sp.を主とする湖沼生の珪藻化石が産出し，輪島層の一部に湖沼成堆積物が存在することが明らかとなった．

(2) 塚田層からは*Denticulopsis praedimorpha*帯（NPD5B帯）上部の区間NPD5B3に属する海生珪藻化石が産出することから，本層の年代は12.3–11.6 Maと推定される．

(3) 塚田層の基底に明瞭な不整合が存在し，輪島層と

第2表　輪島市気勝平町ルートの珪藻化石産出表.

Table 2　Occurrence chart of diatoms in the Kekachidairamachi route, Wajima City.

Formation	\ Tsukada Formation																				
Diatom zones	*Denticulopsis praedimorpha* Zone (NPD5B)																				
Sample number (K)	01	02	03	04	05	06	07	08	09	10	11	12	13	14	15	16	17	18	19	20	21
Original sample number (Noto)	1359	1358	1357	1356	1355	1354	1353	1352	1351	1350	1349	1348	1347	1346	1344	1345	1360	1361	1362	1363	1364
Preservation	M	M	M	M	M	P	G	M	M	M	M	M	M	P	M	M	M	P	P	M	M
Abundance	C	C	A	C	C	R	A	C	C	C	C	C	C	C	C	C	C	C	C	C	C
Marine diatoms																					
Actinocyclus ingens f. *ingens* (Rattray) Whiting et Schrader	4	3	+	1	-	2	+	10	8	+	+	2	6	17	4	3	+	2	8	4	2
A. octonarius Ehr.	-	+	1	1	-	-	-	-	-	1	-	3	1	-	-	-	-	2	-	-	-
A. sp. A	-	-	-	-	-	-	-	-	-	-	-	-	-	1	-	-	-	-	-	+	-
Actinoptychus senarius (Ehr.) Ehr.	1	1	1	-	+	1	+	+	1	+	+	4	-	1	2	2	3	4	1	2	3
A. vulgaris Schum.	+	-	-	-	-	-	-	-	-	-	-	-	-	-	-	-	-	-	-	-	-
Arachnoidiscus spp.	-	-	-	-	-	-	-	-	-	-	-	-	-	-	-	-	-	-	-	1	-
Azpeitia endoi (Kanaya) P.A.Sims et G.A.Fryxell	3	6	1	6	2	1	1	+	-	1	1	2	-	1	1	1	2	2	-	-	+
A. cf. *nodulifera* (A.W.F.Schmidt) G.A.Fryxell et P.A.Sims	-	+	-	-	-	1	+	-	-	-	-	1	-	-	-	-	-	-	-	-	-
A. vetustissima (Pant.) P.A.Sims	16	+	2	1	2	-	-	-	1	+	-	-	-	-	1	-	-	2	-	-	-
*Cavitatus jouseanus (*Sheshukova*)* D.M.Williams	+	-	-	-	-	-	-	-	-	-	-	-	-	-	+	-	-	-	-	-	-
C. miocenicus (Schrader*)* Akiba et Yanagisawa	-	-	-	1	-	+	-	-	-	-	-	-	-	-	+	-	-	-	-	-	-
Cocconeis californica Grunow	-	-	-	-	-	-	-	-	-	-	1	-	-	-	-	-	-	-	-	-	-
C. costata Greg.	-	-	-	-	-	-	1	-	-	-	-	-	-	-	1	-	-	-	-	-	-
C. scutellum Ehr.	-	-	-	-	-	-	-	-	-	-	-	-	-	-	-	-	-	-	1	-	-
C. vitrea Brun	+	-	-	-	-	3	+	+	-	+	-	+	+	-	-	1	-	-	6	-	+
Coscinodiscus marginatus Ehr.	+	1	1	+	1	1	1	1	1	2	5	2	3	3	1	2	1	+	2	5	2
C. spp.	+	1	-	+	-	-	2	-	2	-	1	1	-	-	-	-	-	-	-	1	-
Cymatosira debyi Temp. et Brun	-	-	-	-	-	-	-	-	-	-	-	-	-	-	-	-	-	-	-	2	-
C. sp.	-	-	-	-	-	-	-	-	-	-	-	-	-	-	-	-	-	-	-	2	-
Delphineis surirella (Ehr.) G.W.Andrews	-	+	-	-	-	-	-	-	-	+	+	-	-	-	-	-	-	-	+	-	-
Denticulopsis hyalina (Schrader) Simonsen	-	-	-	-	-	-	-	-	+	-	-	-	-	-	-	-	-	-	-	-	-
D. praedimorpha var. *minor* Yanagisawa et Akiba (Closed copula)	-	-	-	+	+	-	-	+	-	-	1	-	+	-	1	-	-	+	-	1	1
D. praedimorpha var. *praedimorpha* Barron ex Akiba (Closed copula)	-	-	1	1	2	+	2	+	2	5	1	3	5	-	-	6	1	2	2	5	-
	+	+	+	+	1	+	+	+	2	10	2	1	1	+	1	7	8	+	1	9	1
D. simonsenii Yanagisawa et Akiba	+	1	+	2	3	2	1	3	3	1	4	-	5	-	+	1	1	2	2	1	+
D. vulgaris (Okuno) Yanagisawa et Akiba	1	5	+	2	2	2	+	2	3	1	2	1	4	1	+	1	-	+	1	1	+
S-type girdle view of *D. simonsenii* group	1	1	1	4	4	6	2	4	8	3	7	1	3	-	1	1	+	+	1	1	-
Diploneis bombus Ehr.	-	-	-	-	-	-	+	-	-	-	-	-	-	-	-	-	-	-	-	1	+
D. smithii (Bréb.) Cleve	-	-	1	-	1	-	1	-	+	1	-	+	1	-	+	-	+	1	+	1	1
Goniothecium rogersii Ehr.	-	-	-	-	-	-	-	-	-	-	-	-	-	-	1	-	1	-	-	-	-
Grammatophora spp.	+	-	-	+	-	+	1	+	-	+	+	+	+	-	+	-	+	+	-	1	+
Hyalodiscus obsoletus Sheshukova	+	1	-	+	1	2	3	+	-	+	1	+	-	1	+	1	5	1	2	-	+
Ikebea tenuis (Brun) Akiba	-	5	-	-	-	+	1	+	-	-	-	-	2	-	-	-	3	-	+	-	-
Mastogloia splendida (Grev.) Cleve	-	-	-	-	-	-	-	-	-	+	-	-	-	-	-	-	-	-	-	-	-
Melosira sol (Ehr.) Kützing	-	-	-	-	-	-	-	-	-	-	1	-	1	-	1	1	-	-	1	2	+
Navicula spp.	-	-	1	-	+	-	+	-	-	-	-	-	-	-	-	-	-	-	-	1	-
Nitzschia grunowii Hasle	-	-	+	-	-	+	2	-	-	-	-	-	-	-	2	-	-	-	-	-	-
N. heteropolica Schrader	+	+	+	+	-	+	+	+	1	+	-	-	-	-	-	-	-	-	-	-	-
N. rolandii Schrader emend. Koizumi	-	-	-	-	-	-	-	-	-	+	-	-	-	-	-	-	-	-	-	-	-
Odontella aurita (Lyngb.) J.A.Agardh	-	-	-	-	-	-	-	-	-	-	1	-	1	-	1	1	-	-	1	2	+
Paralia sulcata (Ehr.) Cleve	3	3	4	+	2	1	6	1	5	18	9	15	9	7	3	7	9	5	6	12	23
Plagiogramma staurophorum (Greg.) Heib.	-	-	-	1	-	-	-	+	-	-	1	-	3	1	-	1	-	+	-	2	-
Proboscia alata (Bright.) Sundstöm	-	-	1	+	-	-	+	-	-	-	-	-	-	-	-	-	-	-	-	-	-
P. barboi (Brun) Jordan et Priddle	1	1	-	-	+	+	-	1	1	-	-	+	-	-	1	-	+	1	-	-	-
Pseudodimerogramma elliptica Schrader	-	-	-	-	-	-	+	-	-	-	-	-	-	-	-	-	-	-	-	-	-
Rhabdonema japonicum Temp. et Brun	-	-	-	-	-	-	+	-	-	-	-	-	-	-	-	-	-	-	-	-	-
Rhizosolenia hebetata f. *hiemalis* Gran	+	2	+	-	-	1	+	+	1	-	-	-	-	-	1	1	3	+	-	-	-
R. miocenica Schrader	-	-	-	-	-	-	-	-	-	-	1	-	-	-	-	-	-	-	-	-	-
R. styliformis Brightw.	+	1	1	+	-	-	-	-	-	-	-	-	-	-	-	1	-	-	1	-	1
R. sp. C	-	-	-	1	-	-	-	-	-	-	-	-	-	-	-	-	-	-	-	-	-
Rouxia californica Perag.	-	+	+	-	-	-	+	+	-	-	-	-	-	-	-	+	-	-	-	-	-
R. peragari Brun et Hérib.	-	-	+	-	-	-	+	-	-	-	-	-	-	-	-	-	-	-	-	-	-
Stellarima microtrias (Ehr.) Hasle et P.A.Sims	+	+	2	-	1	+	-	1	+	+	-	-	1	-	-	-	-	-	-	-	-
Stephanogonia hanzawae Kanaya	+	+	+	-	+	1	-	-	-	+	-	-	-	-	-	-	1	+	1	-	-
Stephanopyxis spp.	-	+	1	-	-	-	-	-	-	2	1	1	1	1	2	2	+	+	3	+	2
Thalassionema hirosakiensis (Kanaya) Schrader	1	+	9	5	14	8	10	4	-	+	-	-	1	1	2	-	-	2	2	-	-
T. nitzschioides (Grunow) H. Perag. et Perag.	19	17	16	20	5	16	13	18	8	10	3	10	6	11	22	16	16	17	7	3	4
T. nitzschioides (heteropolar)	-	-	1	+	-	-	-	-	-	-	-	-	-	-	-	-	-	-	-	-	-
Thalassiosira grunowii Akiba et Yanagisawa	+	1	-	+	-	-	+	+	3	+	-	-	-	-	3	1	-	3	-	-	-
T. leptopus (Grunow) Hasle et G.A.Fryxell	-	-	-	-	-	-	-	-	-	-	-	-	-	1	1	+	-	+	-	-	+
T. praenidulus Akiba	-	-	-	4	-	-	-	-	-	2	1	-	-	-	-	-	-	1	-	-	-
Triceratium condecorum Brightw.	-	+	-	-	-	-	-	-	-	-	-	-	-	-	-	-	+	-	-	-	-
Non-marine diatoms																					
Actinocyclus sp.	-	-	-	-	-	-	-	-	-	-	-	1	-	-	-	-	-	-	-	-	-
Aulacoseira spp.	+	+	5	+	9	2	3	4	2	1	11	4	2	4	1	-	4	3	3	2	11
Total number of valves counted	50	50	50	50	50	50	50	50	50	50	50	50	50	50	50	50	50	50	50	50	50
Resting spore of *Chaetoceros*	19	23	34	11	15	34	17	10	12	39	11	11	12	2	24	9	14	26	25	18	18

塚田層の堆積期の間，輪島市の内陸を含む能登半島西部
は陸域が存在していたと推定される．

文　献

Akiba, F.（1986）Middle Miocene to Quaternary diatom biostratigraphy in the Nankai Trough and Japan Trench, and modified Lower Miocene through Quaternary diatom zones for middle-to-high latitudes of the North Pacific. *In* Kagami, H., Karig, D. E., Coulbourn, W. T. *et al.*, *Initial Report of Deep Sea Drilling Project*, **87**, 93–480.

Fuji, N.（1972）Fossil spores and pollen grains from the Neogene deposits in Noto Peninsula, central Japan – IV A palynological study of the Late Miocene Tsukada Member. *Transactions and Proceedings of the Palaeontological Sosiety of Japan, New Series*, no. 86, 295–318.

Gradstein, F., Ogg, J. Schmitz, M. D. and Ogg, G. M.（2012）*A Geologic Time Scale 2012*. Cambridge Univ. Press, Cambridge, 1144p.

市川　渡・絎野義夫(1963)　能登半島の珪藻土．石川県，45p.

上　俊二・加藤道雄・田口恭子・高山俊昭(1981)　能登半島に分布する石灰質砂岩層の地質年代．金沢大学教養部論集　自然科学篇，**18**，47–63.

絎野義夫編(1965)　第1部　能登半島の地質．能登半島学術調査報告書，石川県，1–93.

絎野義夫編著(1993)　石川県地質誌．石川県・北陸地質研究所，321p.

小林博文・山路　敦・増田富士雄(2005)　能登半島輪島地域の中新統の層序・堆積環境・テクトニクス．地質学雑誌，**111**，286–299.

Okada, H. and Bukry, D.（1980）Supplementary modification and introduction of code numbers to the low-latitude coccolith biostratigraphic zonation (Bukry, 1973; 1975). *Marine Micropaleontology*, **5**, 321–325.

奥野春雄(1973)　1　ケイ藻・ケイ藻土・地の粉．輪島市史：資料編，725–782.

Watanabe, M. and Yanagisawa, Y.（2005）Refined Early Miocene to Middle Miocene diatom biochronology for the middle- to high-latitude North Pacific. *Island Arc*, **14**, 91–101.

柳沢幸夫(1999)　能登半島珠洲地域の中新統の珪藻化石層序．地質調査所月報，**50**，167–213.

柳沢幸夫(2012)　石川県輪島市（能登半島）に分布する中新統塚田泥岩層の珪藻化石．地質調査総合センター研究資料集，no. 567，1–9.

柳沢幸夫(2013)　輪島塗の下地に使用される珪藻土の秘密．漆サミット実行委員会編，漆サミット 2013in輪島―漆文化と漆産業の再興を目指して―，9.

Yanagisawa, Y. and Akiba, F.（1998）Refined Neogene diatom biostratigraphy for the northwest Pacific around Japan, with an introduction of code numbers for selected diatom biohorizons. *Journal of Geological Society of Japan*, **104**, 395–414.

吉川敏之・鹿野和彦・柳沢幸夫・駒澤正夫・上嶋正人・木川栄一(2002)　珠洲岬，能登飯田及び宝立山地域の地質．地域地質研究報告(5万分の1地質図幅)，産業技術総合研究所地質調査総合センター，76p.

図版 1　輪島層から産出した非海生珪藻化石.

Plate 1　Non-marine diatoms from the Wajima Formation.

　　1–5: *Actinocyclus* sp.
　　　　1: M07（Noto1377）; 2, 4: M09（Noto1375）; 3, 5: M06（Noto1368）

　　6: *Tetracyclus ellipticus* var. *lancea* f. *subrostrata* Hustedt
　　　　M07（Noto1377）

　　7: *Tetracyclus* sp.
　　　　M06（Noto1368）

　　8–12: *Aulacoseira* spp.
　　　　M09（Noto1375）

　　13–19: *Aulacoseira hachiyaensis* H.Tanaka
　　　　13, 16: M09（Noto1375）; 14, 15: M07（Noto1377）; 17–19: M06（Noto1368）
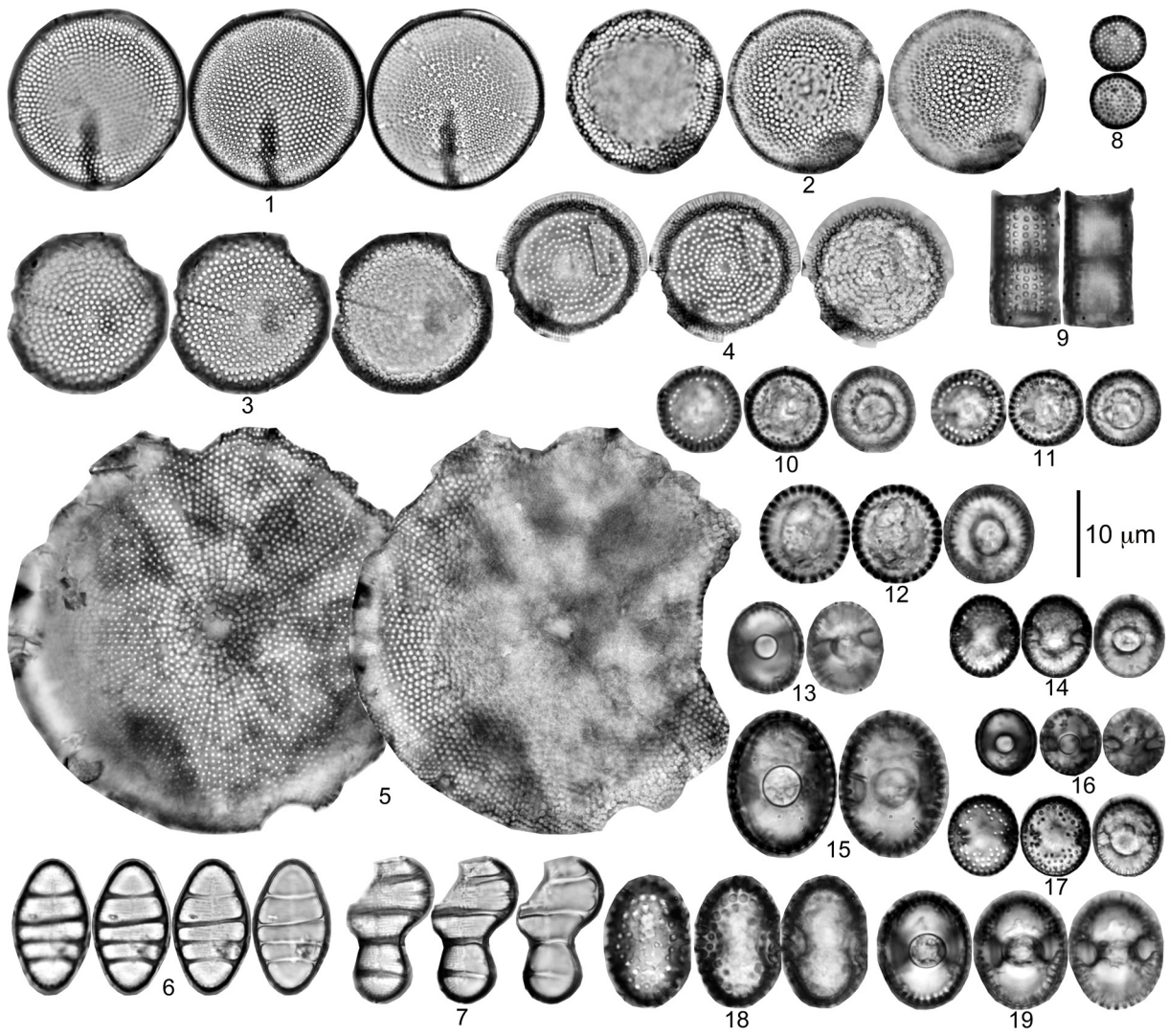
図版 2　塚田層から産出した海生珪藻化石．スケール A は 1–10 に，スケール B は 11–22 に適用．

Plate 2　Marine diatoms from the Tsukada Formation. Scale bars A and B are for figs. 1–10 and 11–22, respectively.

1–3: *Denticulopsis praedimorpha* var. *praedimorpha* Barron ex Akiba [valves], M21 (Noto1365)

4: *Denticulopsis praedimorpha* var. *minor* Yanagisawa et Akiba [valve], K07 (Noto1353)

5, 6: *Denticulopsis praedimorpha* var. *minor* Yanagisawa et Akiba [closed copula], M21 (Noto1365)

7, 8: *Denticulopsis praedimorpha* var. *praedimorpha* Barron ex Akiba [closed copula], M21 (Noto1365)

9: *Denticulopsis simonsenii* Yanagisawa et Akiba, K07 (Noto1353)

10: *Denticulopsis vulgaris* (Okuno) Yanagisawa et Akiba, K07 (Noto1353)

11: *Proboscia alata* (Brightw.) Sundstöm, K07 (Noto1353)

12: *Rhizosolenia styliformis* Brigthw., K07 (Noto1353)

13: *Rhizosolenia hebetata* f. *hiemalis* Gran, K07 (Noto1353)

14: *Ikebea tenuis* (Brun) Akiba, K07 (Noto1353)

15, 16: *Thalassionema hirosakiensis* (Kanaya) Schrader, K07 (Noto1353)

17: *Nitzschia heteropolica* Schrader, K07 (Noto1353)

18, 19: *Actinocyclus* sp. A, K07 (Noto1353)

20: *Azpeitia endoi* (Kanaya) P.A.Simis et G.A.Fryxell, K07 (Noto1353)

21: *Azpeitia vetustissima* (Pant.) P.A.Sims, K07 (Noto1353)

22: *Genus* et sp. indet., K07 (Noto1353)

Article
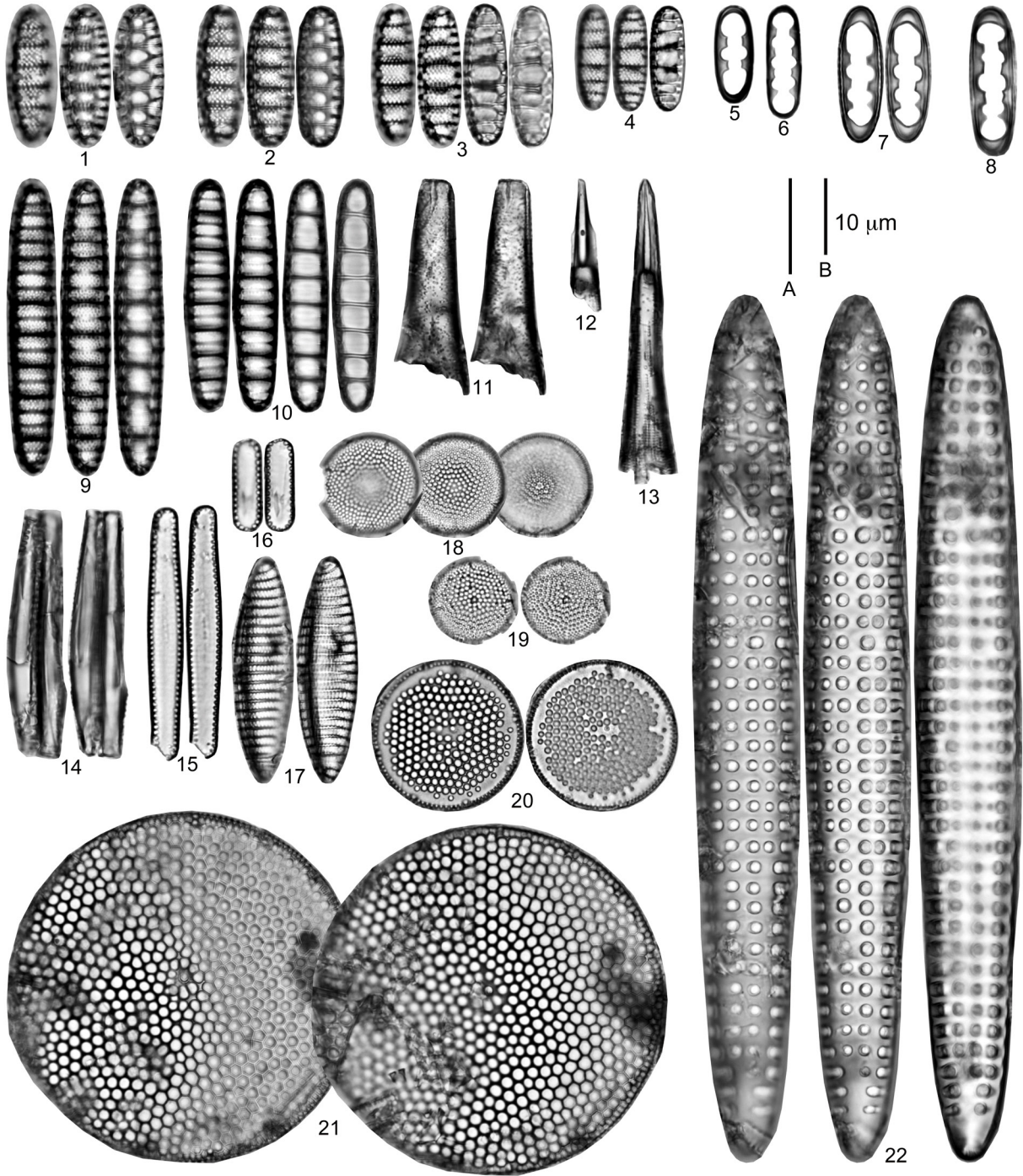
The cause of the east–west contraction of Northeast Japan

Masaki Takahashi[1,*]

Abstract: Northeast (NE) Japan, where the Pacific Plate is subducted to the west, frequently suffers large earthquakes not only along the Japan Trench but also along the Japan Sea side. Those occurred in the former area (subduction–zone earthquake) such as the 2011 off the Pacific coast of Tohoku Earthquake can easily be understood as a releasing process of accumulated stress along the boundary between the subducting Pacific Plate and the overlying plate. On the contrary, those in the latter area (inland earthquake), which occur at relatively shallow depth (<20 km), cannot be explained by such a simple dislocation model. Here I show, the cause of such inland earthquakes can be identified by considering the plate kinematics around the Japanese Islands on the basis of three dimensions, not conventional two dimensions, and the cause of the present E–W contractive tectonics of NE Japan is not the Pacific Plate motion itself but the northwestward–moving Philippine Sea Plate.

1. Introduction

It is well known that the Japanese Islands are currently situated under E–W compression stress field (Terakawa and Matsu'ura, 2010). The E–W contraction causes segmentation of the upper crust of NE Japan separated by a large number of N–S trending reverse faults, which results in its topography (Okamura *et al*., 1995; Sato, 1989; Sato, 1994; Sato *et al*., 2002). The Niigata Prefecture Chuetsu Earthquake (Mw = 6.6) in 2004 is a typical example of the inland earthquakes generated by such crustal deformation. Most of the Japanese earth scientists consider that a relatively rapid Pacific Plate motion of 9–10 cm/year to the west (Demets *et al*., 2010) is the cause of the E–W contractive tectonics (Ikeda, 2012). However, there is a fatal problem in the idea.

If we assume the contraction of NE Japan as an elastic deformation, the accumulated stress acting on the inland arc crust will be reset to the initial state once a large subduction–zone earthquake occurs. On the other hand, when we treat NE Japan as a viscoelastic body, its topographic growth would be reproduced as an inter–seismic plastic deformation. But the geological investigation revealed that the E–W contractive tectonics started at about 3 Ma after tectonically calm state of more than 10 million years (Sato, 1994) while the motion of the Pacific Plate has been almost constant for more than past

40 million years (Harada and Hamano, 2000). Therefore, suppose the E–W contraction of NE Japan is caused by the Pacific Plate motion itself, the Japanese Islands should have been contracted at least for 15 million years after the Japan Sea opening, a hypothesis which is promptly dismissed by the geological evidence. The mpeg-4 movie of the thought–experiment for the cause of the E–W contraction of NE Japan is also presented to make it easier to understand (Takahashi, 2017). Analog models are used for help the comprehension through this work.

The Japanese Islands except the eastern Hokkaido locate on the eastern margin of the Eurasian Plate, under which both the Pacific and Philippine Sea Plate are subducted (Fig. 1), and the relative motion of these three tectonic plates is considered to trigger large earthquakes in the region. The Philippine Sea Plate moves northwestward and is subducted beneath Southwest (SW) Japan along the Nankai Trough at a velocity of 4 cm/year (Seno *et al*., 1993), while the Pacific Plate moves to the west at a velocity of 9–10 cm/year (Demets *et al*., 2010) and is subducted underneath of NE Japan along the Japan Trench. The Pacific Plate is also subducted under the Philippine Sea Plate along the Izu–Ogasawara Trench. Three plates and three plate boundaries (trenches) meet at a point offshore central Japan, which is called a trench–trench– trench (T–T–T) triple junction. The geometric stability of the T–T–T triple junction is the key to solve the riddle.

[1] AIST, Geological Survey of Japan, Research Institute of Geology and Geoinformation

[*] Corresponding author: M. Takahashi,Central 7,1-1-1 Higashi, Tsukuba, Ibaraki 305-8567, Japan. Email: msk.takahashi@aist.go.jp
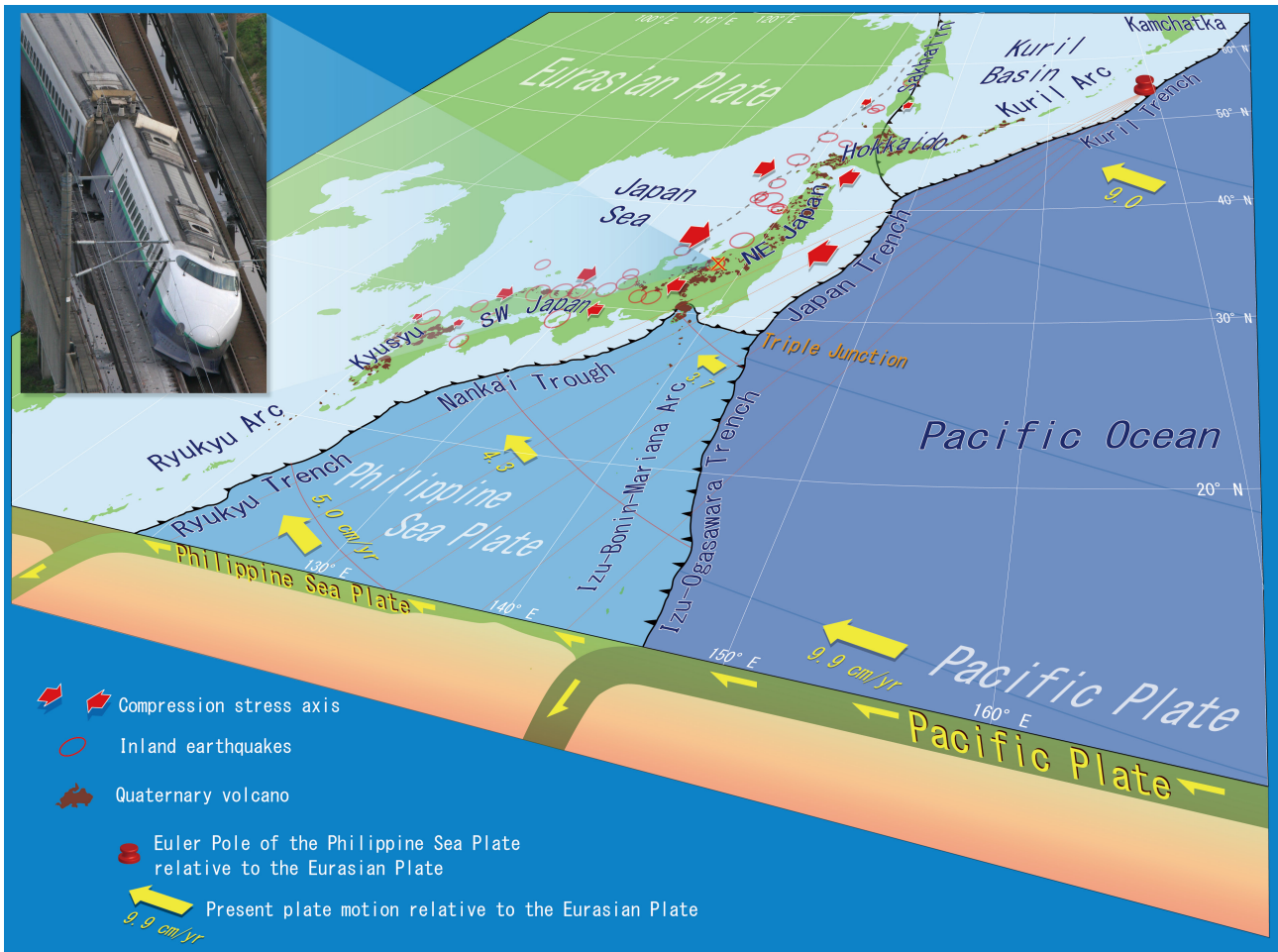
Fig. 1 Tectonic setting of the Japanese Islands. A number of large earthquakes occur particularly along the Japan Sea side of NE Japan. A high–speed train (Shinkansen) was derailed in the Niigata Prefecture Chuetu Earthquake occurred on Nov. 23, 2004 (Photo by the Yomiuri).

2. Analog model experiment

2.1 Initial model

An analog model is very helpful in visual comprehension of the relationship between the three plates around Japan (Takahashi, 2017). At the beginning, two–dimensional plate kinematics is reproduced using the model (Fig. 2), which is composed of three parts: a wooden board (Base Board), and two transparent acrylic sheets which correspond to the Philippine Sea Plate (Sheet A) and the Eurasian Plate (Sheet B). The Sheet A is pinned at the present Euler Pole of the Philippine Sea Plate (a red pin in Fig. 2) located to the northeast of Hokkaido (Seno *et al.*, 1993), so that it can rotate around the pole. The Sheet B is laid over the Sheet A and fixed to the Base Board. This model, in which Japanese Islands are assumed as a part of stable Eurasian Plate and never be deformed, can simply reproduce the motion and subduction of the Philippine Sea Plate.

The geometric transition of the three plates from the present to 12 million years later is illustrated in Fig. 3.

The Japan Trench is fixed in place throughout the period, whereas the Izu–Ogasawara Trench migrates westward as the Philippine Sea Plate rotates. Thereby, the Japan Trench and the Izu–Ogasawara Trench are pulled apart from each other, generating a transform fault that connects these two separating trenches. The length of the transform fault increases with time. The moment the Izu–Ogasawara Trench moves away from the Japan Trench, the T–T–T triple junction becomes another type, a T–T–F (transform fault) triple junction. This is the reason why the present T–T–T triple junction offshore central Japan is regarded as a geometrically unstable condition (McKenzie and Morgan, 1969).

If the two trenches depart from each other, the Pacific Plate should be cut by a tear fault (Fig. 3), forming a right–lateral transform fault between them. Three million years later, the displacement between the two trenches will be 50–60 km based on the present Philippine Sea Plate motion, while the Pacific Plate will travel about 300 km, because it moves to the west at a rate of 10 cm/year. This means that the tear fault will have split the
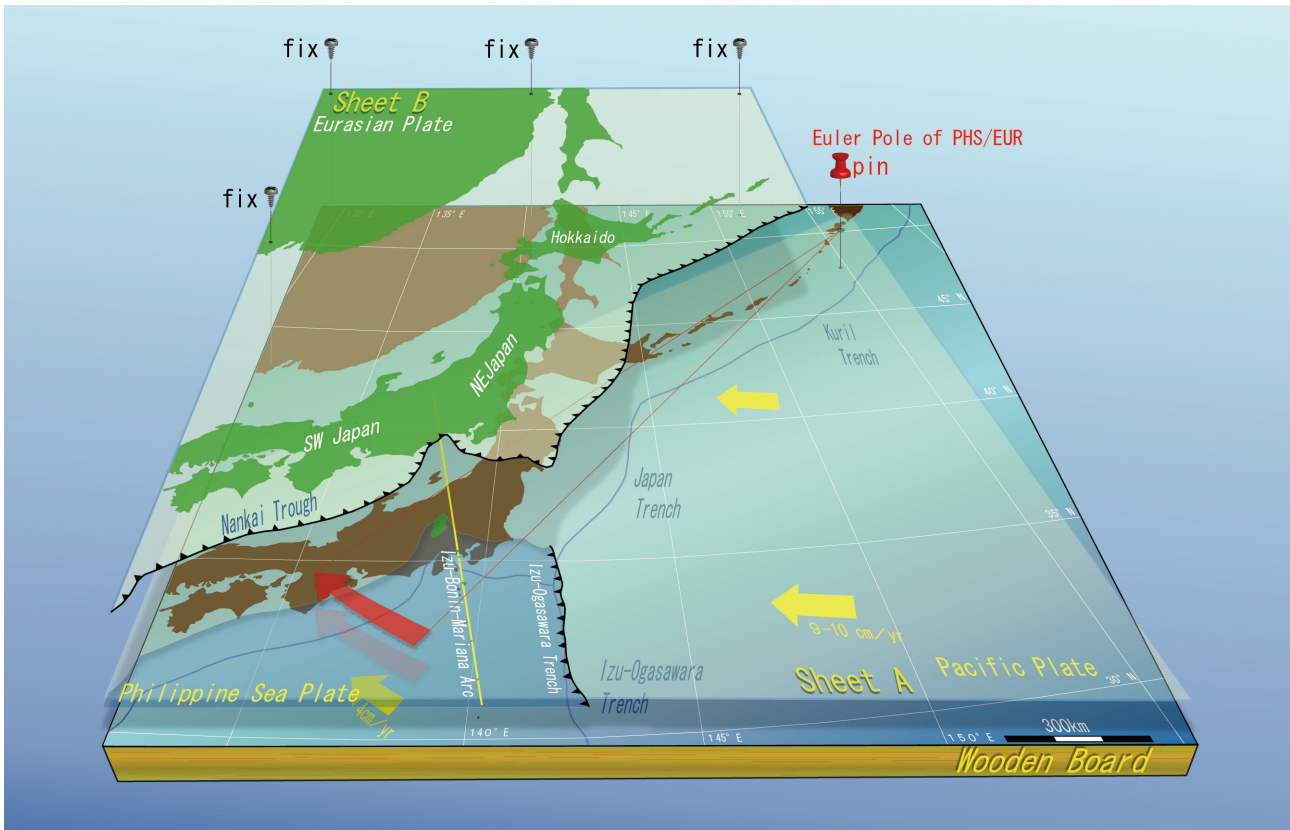
Fig. 2 Initial analog model of the Philippine Sea Plate motion. Overlaying Japanese Islands (NE and SW Japan) are not deformed in this case.
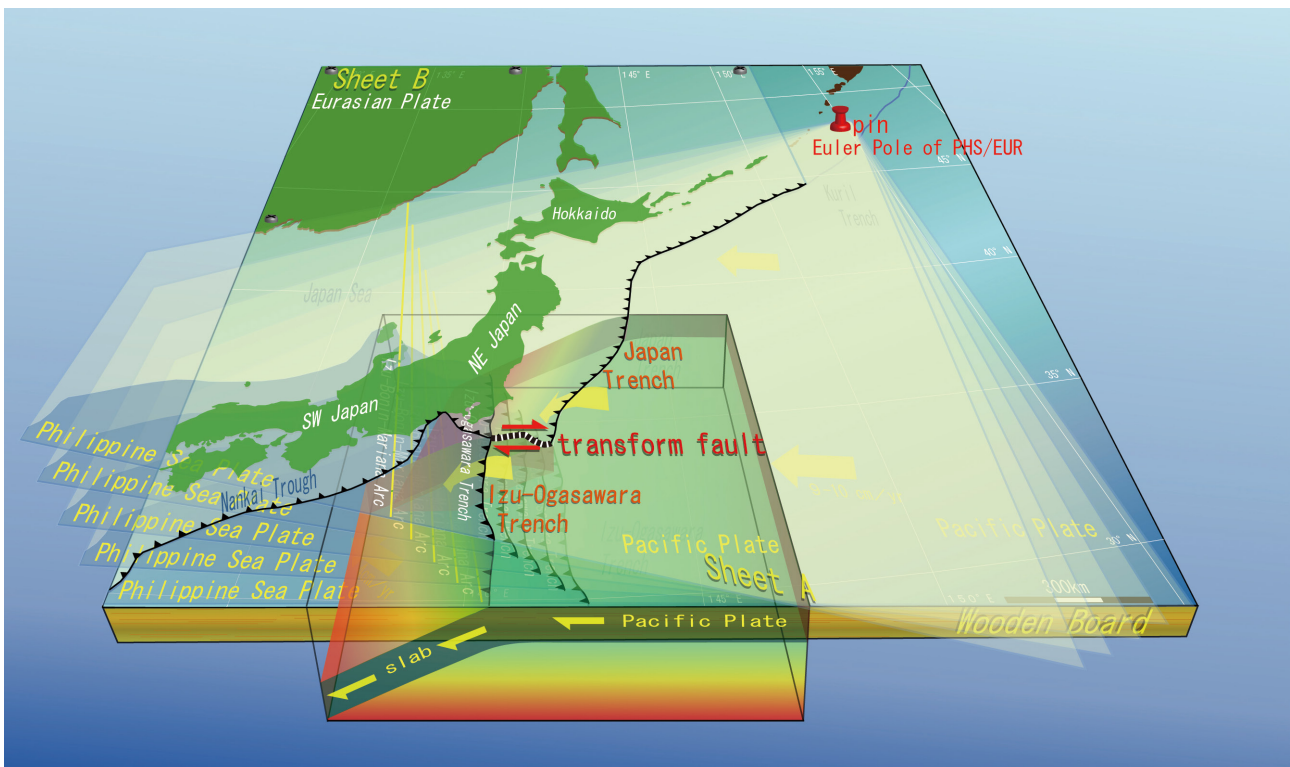
Fig. 3 Three–dimensional geometry of the three plates around the triple junction (present to 12 m.y. future). The subducting Pacific Plate (slab) should be cut by a tear fault, if NE Japan will never be deformed.
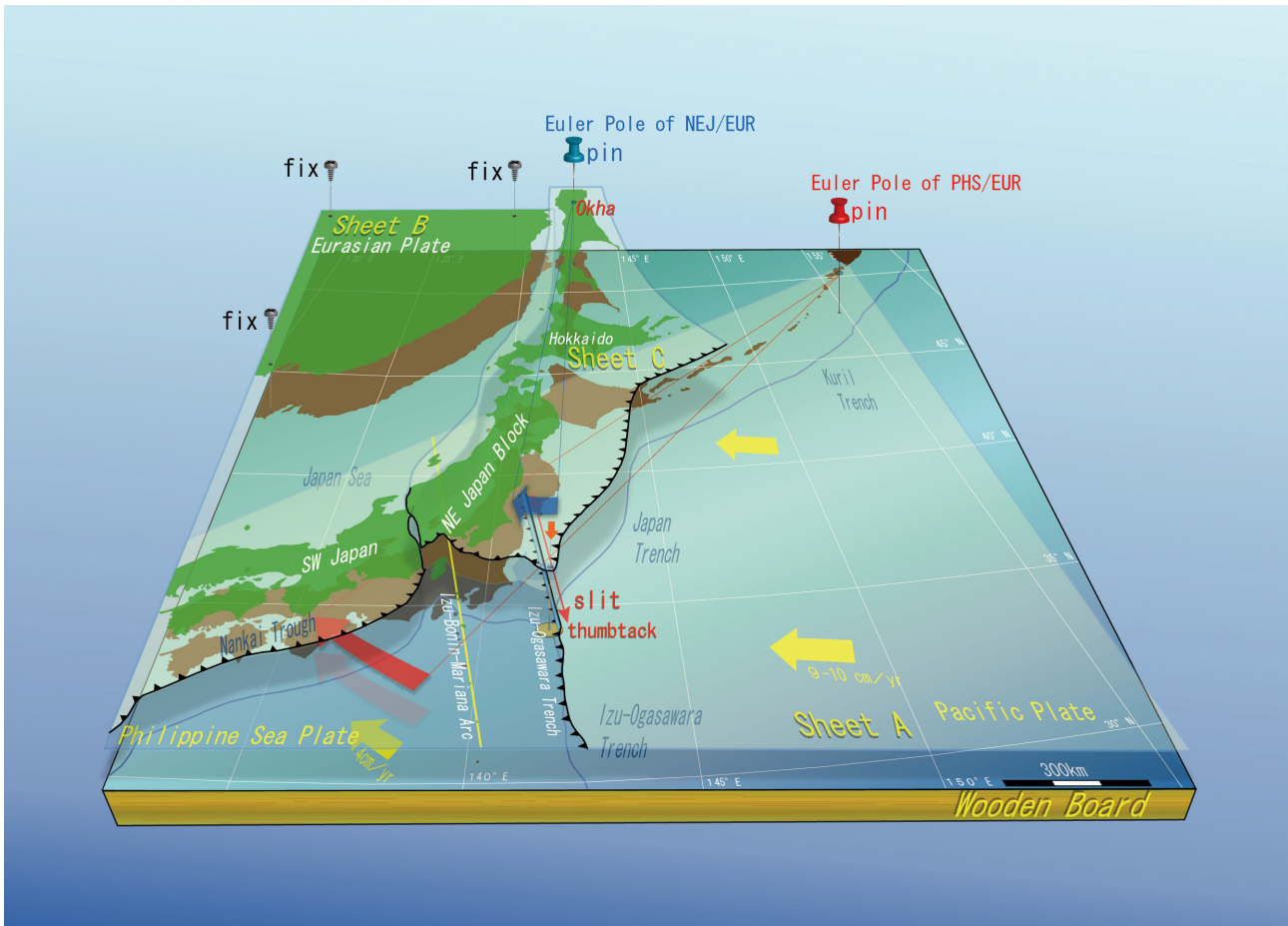
Fig. 4 The Pacific Plate will never be cut by tear fault in this improved model.

Pacific Plate for almost 300 km. However, the Pacific Plate, formed in Jurassic to Cretaceous Periods, is the thickest (about 90 km) and coldest plate on the Earth, so is too rigid to be sheared easily. In fact, the slab of the Pacific Plate is observed to be continuous around the triple junction based on the hypocenter distribution of subduction–zone earthquakes (Nakajima *et al*., 2009). Consequently, it is quite unlikely that the Pacific Plate is to be sheared at the triple junction, i.e., two trenches should be continuous. Therefore, the model should be revised so that the Japan Trench and Izu–Ogasawara Trench can always be continuous under all circumstances.

2. 2   Improved model

The model is taken apart first and a linear slit is cut in the Sheet A along the Izu–Ogasawara Trench (Fig. 4). This corresponds to the subducted part of the trench. Then the Sheet A is pinned at its Euler Pole (shown as a red pin) so that it can rotate about the pole. Second, NE Japan (Sheet C) is cut off from the Sheet B along the eastern margin of the Japan Sea, because it is considered to move independently from the Eurasian Continent. Third, a thumbtack is inserted into the slit from under the bottom of the Sheet A, on which the Sheet B is overlaid.

Only the Sheet B is screwed on the Base Board. Next, the Sheet C is overlaid on the Sheet B, being pierced by the thumbtack at the southern tip of the Japan Trench so that the Japan Trench and the Izu–Ogasawara Trench can move together. Finally, the Sheet C is stuck by a blue pin at northern Sakhalin, because the Euler Pole between NE Japan and stable Eurasian Plate is located near Okha in Sakhalin (Wei and Seno, 1998). The thumbtack moves along the slit as the Philippine Sea Plate rotates, which turns NE Japan clockwise. Now, an unsplit Pacific Plate model, in which two trenches move along with each other, has been completed.

3.   Discussion

In the improved analog model, both the Izu–Ogasawara Trench and triple junction move westward together with the Philippine Sea Plate motion. The Japan Trench, which was immovable in the previous model, also migrates westward because the southern end of the Japan Trench is pierced by the thumbtack of the Philippine Sea Plate sheet (Sheet A in Fig. 5). In this model, the eastern margin of NE Japan corresponds to the Japan Trench, so NE Japan on the Sheet C swings to the west around a pivot at Sakhalin
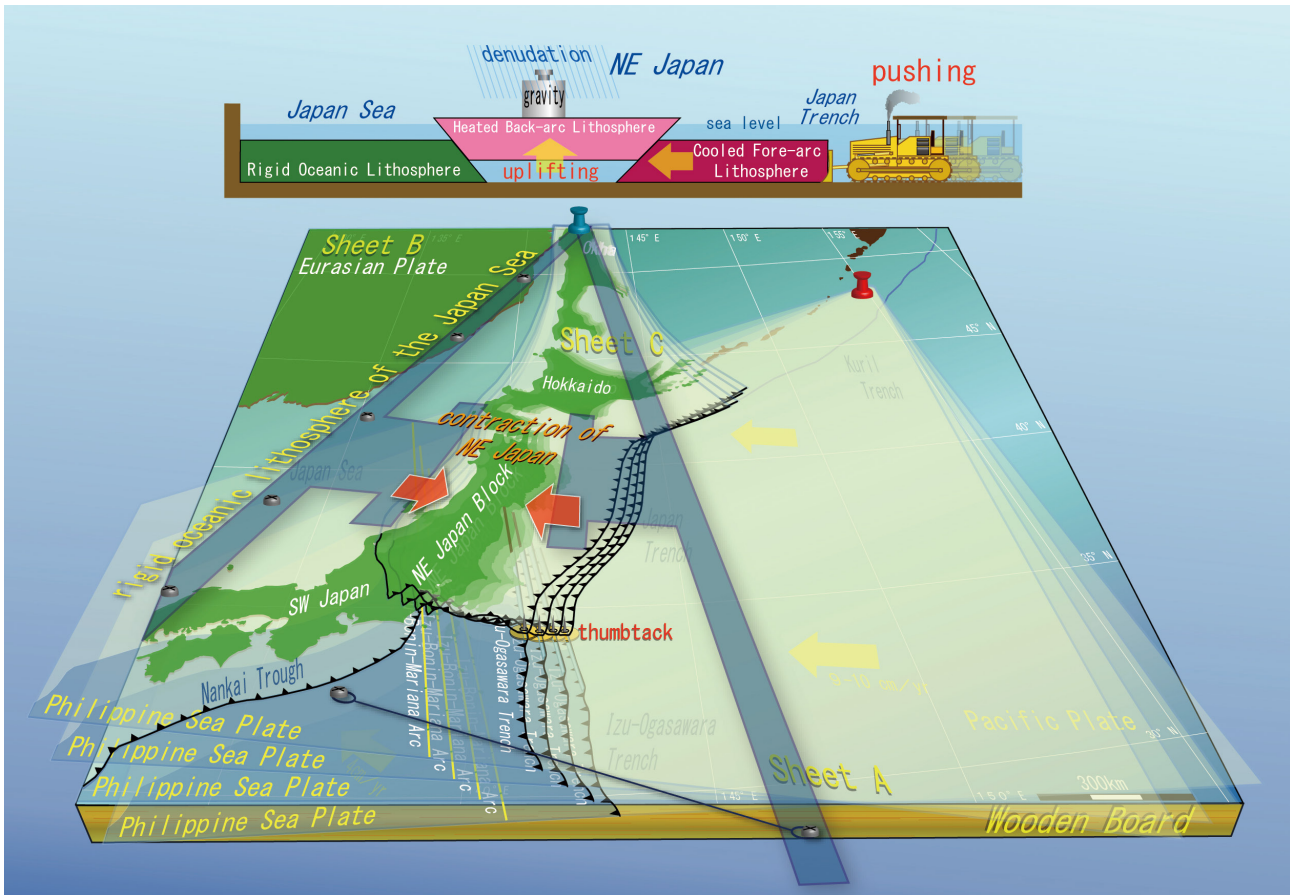
Fig. 5 Geodynamic flame work of the Japanese Islands. NE Japan is contracted like a walnut caught in a nutcracker.

(blue pin in Fig. 4).

The relative velocity of migrating triple junction to stable Eurasia is estimated as 2–3 cm/year based on the present Philippine Sea Plate motion. Therefore, the southern end of the Japan Trench also moves westward at the same speed. The westerly migrating Japan Trench will push the overriding NE Japan to the west, unless whole of its westward motion is cancelled out by tectonic erosion along the Japan Trench (Von Huene and Lallemand, 1990). The arc crust of NE Japan is thus sandwiched between the westerly moving Japan Trench and the rigid and stable oceanic lithosphere of the Japan Sea and then contracted (Fig. 5).

The western half of NE Japan arc crust (back-arc region) has been heated and weakened for a geologically long time by volcanic activity (Yoshida, 2001). In fact, possible deep-seated magmatic activity is imaged in the region by seismic tomography (Hasegawa *et al.*, 1991; Zhao *et al.*, 1992). By contrast, the fore–arc region (Japan Trench side), which has been cooled by the subducting old oceanic lithosphere of the Pacific Plate, is not so deformable. Thus the E–W contraction of NE Japan has been concentrated along the Japan Sea side due to thermo-rheological difference.

Thus, if the Pacific Plate is assumed not to be shorn by a tear fault at the triple junction, and actually it is not, the Philippine Sea Plate motion will cause the Izu–Ogasawara Trench to migrate westward, then T–T–T triple junction, Japan Trench, and NE Japan successively. Thereby, the arc crust of NE Japan has no choice but to shorten its width as it drifts westward. This E–W contraction tectonics causes a number of large inland earthquakes particularly along the back–arc region, far from the plate subduction boundary (Japan Trench). Therefore, the cause of inland earthquakes along the Japan Sea side of NE Japan is the Philippine Sea Plate, not the Pacific Plate. It is the imposed displacement arising from moving subduction boundary of the Pacific Plate (Japan Trench) that causes the E–W contraction of NE Japan, not the Pacific Plate motion itself.

4. Conclusion

Considering the three dimensional kinematics of the Pacific and Philippine Sea Plates relative to the overlying Eurasian Plate, I propose that the present E–W contractive tectonics of NE Japan is brought about by the north–westward motion of the Philippine Sea Plate, not by the Pacific Plate motion itself.

References

Demets, C., Gordon, R. G. and Argus, D. F.（2010）Geologically current plate motions. *Geophys. Jour. Intern.*, **181**, 1–80. doi: 10.1111/j.1365–246X.2009.04491.x.

Harada, Y. and Hamano, Y.（2000）Recent progress on the plate motion relative to hotspots. *In* Rechards, M. A., Gordon, R. G. and Hilst, R. D. V. D. eds., *The History and Dynamics of Global Plate Motions*, *AGU Geophys. Monogr. Ser.*, **121**, 327–338. doi: 10.1029/GM121p0327.

Hasegawa, A., Zhao, D., Hori, S., Yamamoto, A. and Horiuchi, S.（1991）Deep structure of the northeastern Japan arc and its relationship to seismic and volcanic activity. *Nature*, **352**, 683–689. doi: 10.1038/352683a0.

Ikeda, Y.（2012）Strain buildup in the Northeast Japan orogeny with implications for gigantic subduction earthquakes. *Episodes*, **37**, 234–245.

McKenzie, D. P. and Morgan, W. J.（1969）Evolution of triple junction. *Nature*, **224**, 125–133. doi: 10.1038/224125a0.

Nakajima, J., Hirose, F. and Hasegawa, A.（2009）Seismotectonics beneath the Tokyo metropolitan area, Japan: Effect of slab–slab contact and overlap on seismicity. *Jour. Geophys. Res.*, **114**, B08309. doi: 10.1029/2008JB006101.

Okamura, Y., Watanabe, M., Morijiri, R. and Satoh, M.（1995）Rifting and basin inversion in the eastern margin of the Japan Sea. *Island Arc*, **4**, 166–181. doi: 10.1111/j.1440-1738.1995.tb00141.x.

Sato, H.（1989）Degree of deformation of late Cenozoic strata in the Northeast Honshu Arc. *Mem. Geol. Soc. Japan*, no. 32, 257–268 (in Japanese, with English abstract).

Sato, H.（1994）The relationship between late Cenozoic tectonic events and stress field and basin development in northeast Japan. *Jour. Geophys. Res.*, **99 (B11)**, 22261–22274. doi: 10.1029/94JB00854.

Sato, H., Hirata, N., Iwasaki, T., Matsubara, M. and Ikawa, T.（2002）Deep seismic reflection profiling across the Ou Backbone range, northern Honshu Island, Japan. *Tectonophysics*, **355**, 41–52. doi: 10.1016/S0040-1951(02)00133-6.

Seno, T., Stein, S. and Gripp, A.（1993）A model for the motion of the Philippine Sea Plate consistent with NUVEL–1 and geological data. *Jour. Geophys. Res.*, **98**, 17941–17948. doi: 10.1029/93JB00782.

Takahashi, M.（2017）Thought experiment relating to the cause of the E–W contraction of NE Japan. GSJ Open-File Report, no. 638, Geological Survey of Japan, AIST.（18-minutes mpeg-4 movie with English subtitles converted from the Power Point presentation; 720 x 540 pixels, 37.3 MB, accessed 2017-03-23）.

Terakawa, T. and Matsu'ura, M.（2010）The 3-D tectonic stress fields in and around Japan inverted from centroid moment tensor data of seismic events. *Tectonics*, **29**, 1–14. doi: 10.1029/2009TC002626.

Von Huene, R. and Lallemand, S.（1990）Tectonic erosion along the Japan and Peru convergent margins. *Geol. Soc. Am. Bull.*, **102**, 704–720.

Wei, D. and Seno, T.（1998）Determination of the Amurian plate motion. *In* Flower, M. F. J., Chung, S. L., Lo, C. H. and Lee, T. Y. eds., *Mantle Dynamics and Plate Interactions in East Asia*, Geodynamics Series, **27**, 337–346, AGU, Washington D. C.

Yoshida, T.（2001）The evolution of arc magmatism in the NE Honshu arc, Japan. *Tohoku Geophys. Jour. (Sci. Rep. Tohoku Univ., Ser. 5)*, **36**, 131–149.

Zhao, D., Hasegawa, A. and Horiuchi, S.（1992）Tomographic imaging of P and S wave velocity structure beneath northeastern Japan. *Jour. Geophys. Res.*, **97**, 19909–19928. doi: 10.1029/92JB00603.

東北日本の東西短縮テクトニクスの原因

高橋雅紀

要　旨

　大部分がユーラシアプレートに属する日本列島には，南からフィリピン海プレートが，東から太平洋プレートが沈み込んでいる．日本列島のうち，本州(東北日本から西南日本)の広い範囲は東西圧縮応力場におかれ，内陸地震が頻発し，断層運動に伴って山地は隆起し内陸盆地は沈降している．この東西短縮テクトニクスの原因について，3つのプレートの運動と，3つの収束境界(海溝)が一点に集まる海溝型三重会合点の三次元幾何学を組み合わせた思考実験を行った．その結果，これまで，西に移動する太平洋プレートの運動そのものに起因すると考えられてきた東西短縮テクトニクスの原因が，北西に移動するフィリピン海プレートの運動によってコントロールされていることが判明した．すなわち，フィリピン海プレートの運動により三重会合点が西に移動し，追随するように日本海溝も西に移動する．その結果，東北日本も西に移動するが，日本海の海洋リソスフェアに阻まれるため，東北日本の島弧地殻は東西に短縮せざるを得ない．このことは，内陸地震の原因が，太平洋プレートの運動そのものではなく，沈み込み位置(日本海溝)の移動であることを意味している．

Notes and Comments

Field guide of Izu-Oshima Volcano

Takahiro Yamamoto[1,*]

Abstract: Izu-Oshima volcano is an active basaltic stratovolcano in the Izu-Mariana arc, and its last major eruption occurred in 1986. This field guide includes descriptions about the 1986 products, the Miharayama Central Cone, the 1421? product at the southern coast, the 1.7-ka caldera-forming products, the pre-caldera tephra formation and the 2013 lahar.

1. Introduction

Izu-Oshima volcano is an active basaltic stratovolcano that forms the northernmost island (15×9 km) of the Izu-Mariana arc (Fig. 1). The elevation of this island is 764 m a.s.l., but the volcanic edifice height is over 1,000 m from the sea floor. The island consists of highly dissected remnants of three old (Early Pleistocene) volcanoes, which are exposed on the northern and eastern coasts, as well as in the products of Izu-Oshima volcano proper (Isshiki, 1984; Fig. 2). These products cover the older edifices and occupy most of the subaerial portion of the island.

2. Eruption history

Izu-Oshima volcano is composed of lava flows and volcaniclastic rocks of low-K, arc-type tholeiitic olivine basalt and pyroxene-olivine basalt (Kawanabe, 1991). The older edifice of the volcano is called the Senzu Group (Nakamura, 1964) and is made up of phreatomagmatic coarse ejecta and lahar deposits with a small amount of lava flows (Fig. 2). Volcanic activity started at about 40 to 50 ka, and represents the stage of emergence of an island. The younger edifice of the volcano consists of normal subaerial alternations of lava flows and scoria and ash falls. This activity began about 20 ka and marks the stage of continuous growth of a stratovolcano above sea level. The upper unit is subdivided into pre-caldera and syn- and post-caldera deposits (Nakamura, 1964). The pre-caldera deposits are made up of about 100 layers of pyroclastic deposits. The intervals between the layers are presumably 150 years on average. There are many flank volcanoes forming fissures, scoria cones and tuff cones. Zone of the flank vents is elongated in NNW to SSE that reflects a regional stress field.

At about 1.7 ka, after a scoria eruption from the summit
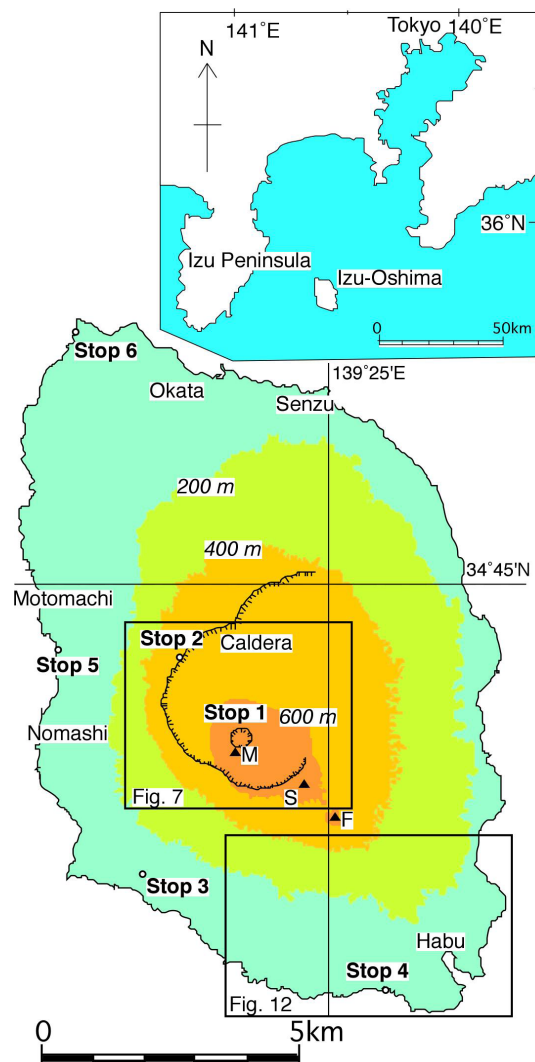
Fig. 1 Index map of Izu-Oshima volcano. M = Miharayama; S = Shiroishiyama; F = Futagoyama

[1] AIST, Geological Survey of Japan, Research Institute of Earthquake and Volcano Geology

[*] Corresponding author: T. Yamamoto, Central 7,1-1-1 Higashi, Tsukuba, Ibaraki 305-8567, Japan. Email: t-yamamoto@aist.go.jp
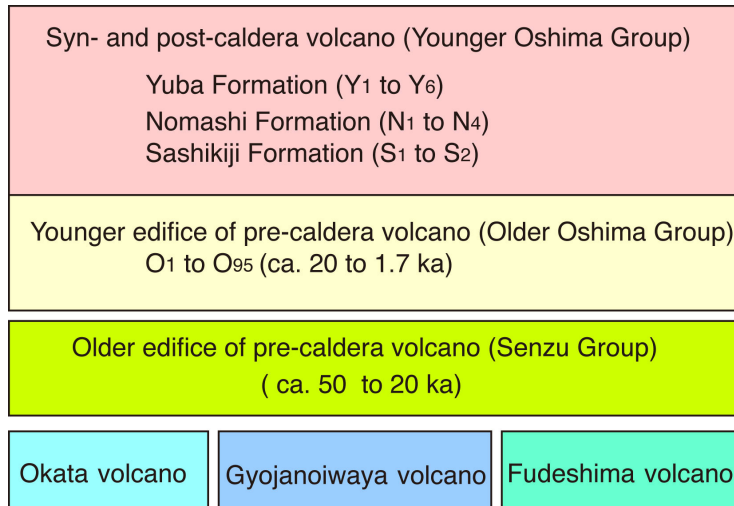
Fig. 2   Geological summary of Izu-Oshima island. Modified from Kawanabe (1998).
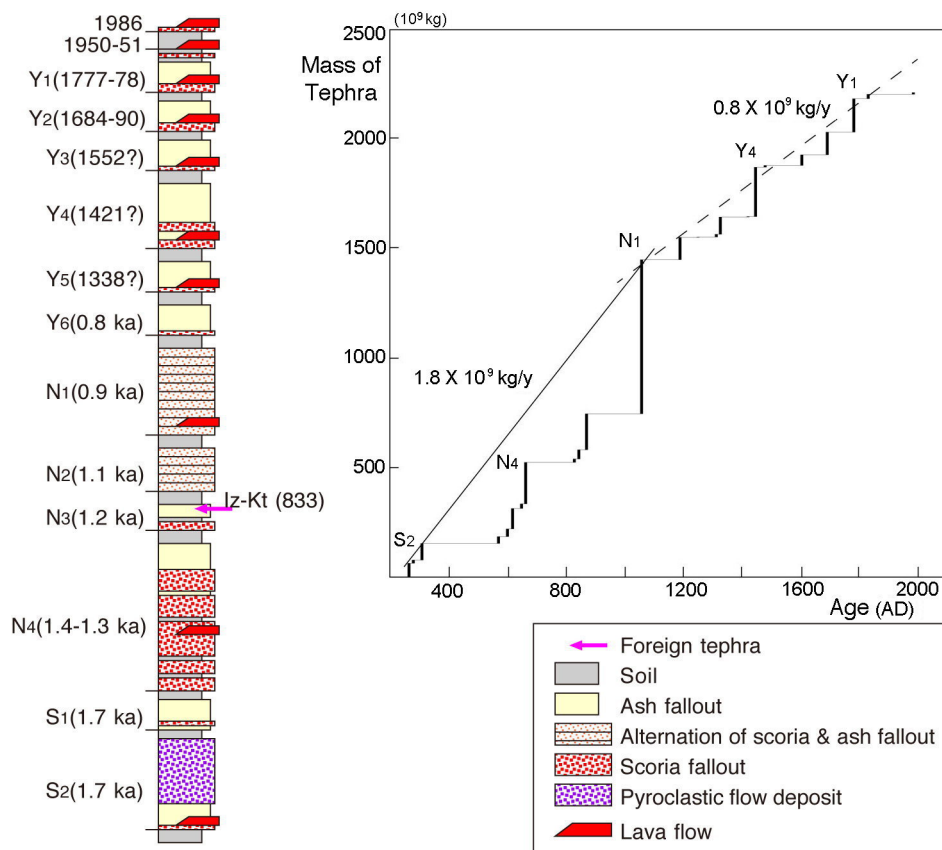
Fig. 3   Stratigraphic section and cumulative mass of tephra for the syn- and post-caldera products of Izu-Oshima volcano. Iz-Kt = Izu-Kozushima-Tenjosan tephra (biotite rhyolite) from Kozushima volcano at AD833. Modified from Kawanabe (1998; 2012).

and several flank eruptions, a large phreatic explosion occurred in the summit area and high-speed pyroclastic density current covered almost all the entire island (Yamamoto, 2006; S_2 in Figs. 2 and 3). The present shape of the summit caldera is thought to be formed in this syn-

caldera stage (Sashikiji Formation; Nakamura, 1964). The post-caldera products are composed of 10 large eruptions and several minor ones (Koyama and Hayakawa, 1996; Kawanabe, 2012). Nakamura (1964) has divided into the Nomashi and Yuba Formations across an erosional contact
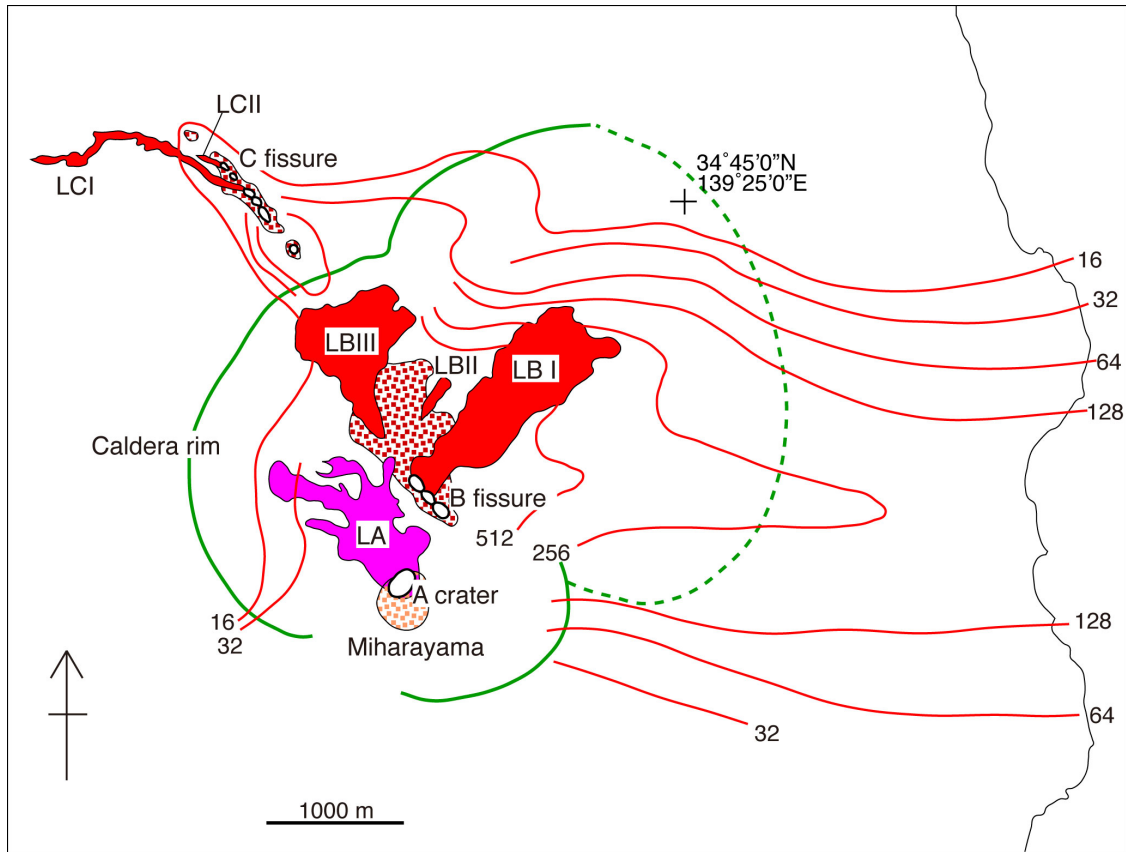
Fig. 4 Distribution of the products of the 1986 eruption. Numerals of each isopach are the thickness of the scoria fall deposits in millimeters. LA, LBI, LBII, LBIII, LCI and LCII are names of lava flows. Hatched areas are scoria cones. Mt Mihara (Miharayama) is the central cone within the summit caldera. Modified from Soya *et al*. (1987).

(Fig. 2). The eruptive volume of these large eruptions is up to a cubic kilometer and the average recurrent interval of the large ones is 100 to 150 years (Fig. 3). The most recent large eruption occurred in 1777–78 (Y$_1$). Large-scale eruptions usually began with scoria fall deposition followed by effusion of lava flows. In some events, flank eruptions took place and caused violent phreatomagmatic explosions near the coast. The emission of phreatic ash from the central cone, Miharayama, followed for several years after the early magmatic activity. After the Y$_1$ eruption, many medium- to small-scale eruptions occurred. The 1876–77, 1912–14, 1950–51 and 1986–87 eruptions were relatively large and erupted several tens million cubic meters of magma.

3. The 1986 eruption

The 1986 event began with a strombolian eruption and basalt lava effusion from the A crater in Miharayama Central Cone on 15 November (Figs. 4 and 5). On 21 November, after a short repose of activity, a fissure eruption occurred with sub-plinian plumes in the northwestern caldera floor (B fissure). The plumes reached 8,000 m height and sprayed scoria fallout on the eastern side. As

Fig. 5 The 1986 strombolian summit eruption from the A crater accompanied by lava flows. Viewed from the NW (Gojinkajaya). Photo by S. Nakano, 21 November 1986.

fissure extended outside the caldera (C fissure) and lava flow (LCI) rushed to the largest town, Motomachi, whole residents and visitors were evacuated out of the island. The ejecta from B and C fissures was andesite, which differed from one of A crater in origin. The eruption itself ceased in the morning of 22 November, but evacuation lasted for about one month. On 16 November 1987,
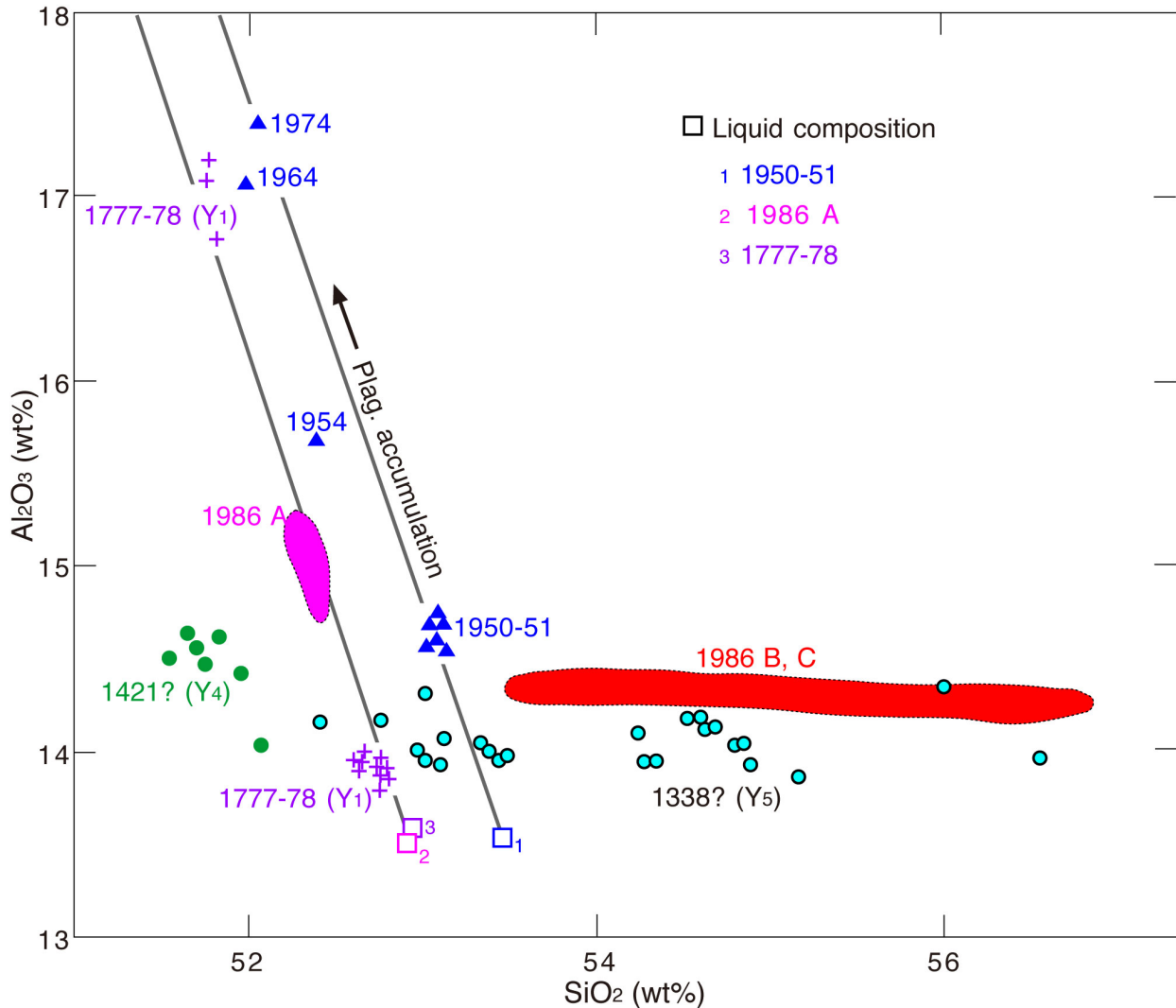
Fig. 6 Al_2O_3 vs. SiO_2 diagram of products of the 1338, 1421, 1777–1778, 1950–1974 and 1986 eruptions; 1986A designates the 1986 summit eruption and 1986B, C the 1986 flank eruption. Three open squares indicate the calculated liquid compositions. Two lines denote respective plagioclase-control lines connected with plagioclase. After Nakano and Yamamoto (1991).

with loud explosions, the lava filling the old pit crater in Miharayama Central Cone were exploded and collapsed. Afterward, several collapses were accompanied by small eruptions, recreating the pit crater in Miharayama. No surface activity, but fumaroles have occurred since the small eruption of 4 October 1990. However, earthquake and volcanic tremor are sometimes observed and a slow inflation of the volcano continues.

4. Geochemistry of the products

The magma of this volcano consists of two types (Nakano and Yamamoto, 1991). One is "plagioclase-controlled" and the other is "differentiated" magma (multimineral-controlled); i.e. the bulk chemistry of the first magma type is controlled by plagioclase addition or removal, while that of the second type is controlled by fractionation of plagioclase, orthopyroxene, clinopyroxene, and titanomagnetite (Fig. 6). Summit eruptions of this volcano tap only plagioclase-controlled magmas, while flank eruptions supply both magma types. It is considered unlikely that both magma types would coexist in the same magma chamber based on the petrology. In the case of the 1986 eruption, the flank magma was isolated from the summit magma chamber or central conduit, and formed small magma pockets, where further differentiation occurred due to relatively rapid cooling. In a period of quiescence prior to the 1986 eruption, new magma was supplied to the summit magma chamber, and the summit eruption began. The dike intrusion or fracturing around the small magma pockets triggered the flank eruption of the differentiated magma.
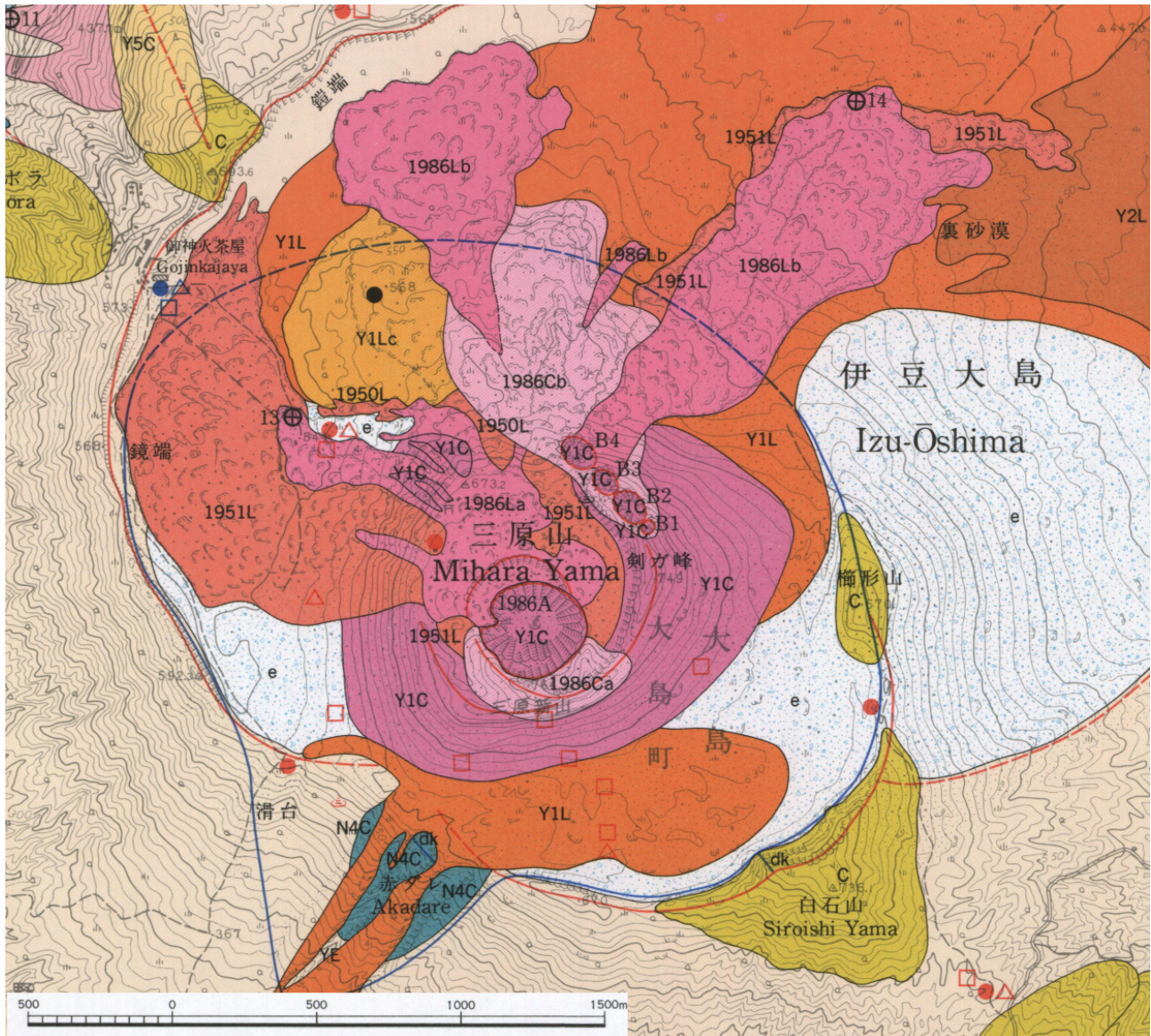
Fig. 7 Geological map around Miharayama Central Cone. Part of the map by Kawanabe (1998).

5. Description of field stops

Stop 1: Hike to Miharayama Central Cone (34.73716˚N, 139.37996˚E to 34.72420˚N, 139.39511˚E)

There is a trail from Gojinkajaya on the caldera-rim to the top of Miharayama. We can observe the 1986, 1950–1951, Y$_1$ (1777–1778) and Y$_2$ (1684) products along this trail (Fig. 7).

The 1986 eruption occurred at the summit from 15 to 23 November (A crater) and at the fissure vents both inside (B fissure) and outside the caldera (C fissure) on 21 November (Fig. 4). The summit lava (1986La) is augite-pigeonite-bronzite basalt, with 6 to 8% plagioclase phenocrysts. Mafic phenocrysts of 1986La total less than 1%. The flank lava (1986Lb and 1986Lc) is nearly aphyric andesite, with rare phenocrysts of plagioclase,

orthopyroxene, clinopyroxene and titanomagnetite, that total less than 1% modally. 1986La is chemically homogeneous throughout the eruption, with 52.2 to 52.5% SiO$_2$ and approximately 15% Al$_2$O$_3$, while flank lavas show a wide variation of SiO$_2$ ranging from 53.5 to 56.9% (Fig. 6). The Al$_2$O$_3$ content of the flank lavas is nearly constant (14.2 to 14.4%), in spite of the SiO$_2$ variation. Temporal variation of the B scoria showed that, initially, scoria compositions were bimodal; i.e. between 53.5 and 53.9% and between 55.3 and 56.1% SiO$_2$. The SiO$_2$-rich scoria was, however, restricted to the initial stage. These temporal compositional variations imply a compositional zonation in the flank magma chamber (Nakano and Yamamoto, 1991).

The 1950–1951 eruption was an intermediate-scale eruption at Miharayama Central Cone similar to the 1986
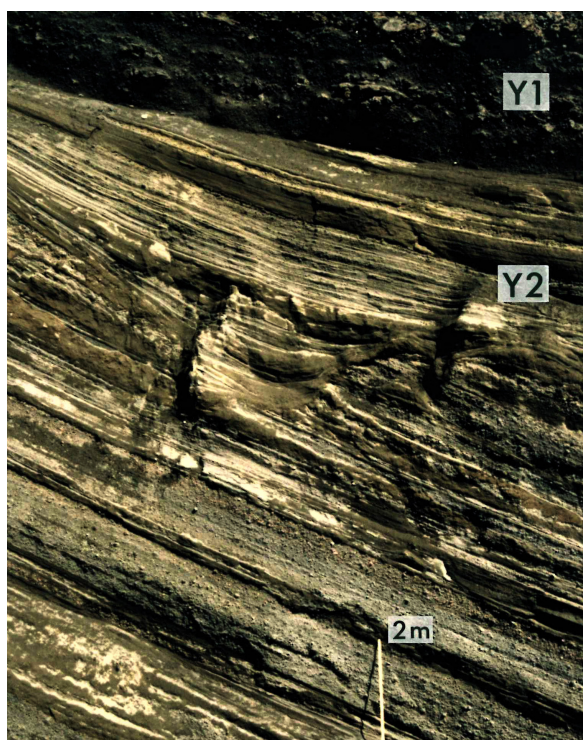
Fig. 8 Phreatomagmatic fallout and surge deposits caused by water inflow into the Miharayama conduit during the magma-withdrawal stage of the Y₂ Member (Y2) at the B2 crater in Miharayama Central Cone (see Fig. 7). Y1 is the basal scoria fall deposit of the Y₁ Member. After Yamamoto (1994). Photo by 15 March 1992.

summit activity from the A crater. Strombolian eruptions and lava effusions took place from the summit crater (Isshiki, 1984). The 1950–1951 lava is augite-bronzite basalt, with 5 to 10% plagioclase phenocrysts, while mafic phenocrysts constitute much less than 1%. The lava is chemically homogeneous with 14.5 to 14.8% $A1_2O_3$ and approximately 53% SiO_2 (Fig. 6).

The Y_1 and Y_2 eruptions were large-scale ones, and Miharayama Central Cone is made up mainly of proximal deposits of Y_1 and Y_2 products. Both consist of basal scoria fall deposit by a sub-plinian eruption and overlying alternation of crossbedded pyroclastic surge and scoria-ash fall deposits (Fig. 8). The overlying unit are called as ash-fall stage deposits, and it is interpreted that the pyroclastic surges was caused by ground water inflow into a conduit during withdrawal of magma (Yamamoto, 1994). The pyroclastic surges expanded about 1 km from the summit vent (blue line in Fig. 7). Duration of main eruption stage, start from basal scoria eject to lava effusion, ranges from 1 to 2 weeks in Y_2 eruption, to 14.5 months in Y_1 eruption. Those of magma-withdrawal stage, ash-fall stage, lasted 6 years in Y_2 and 9 years in Y_1, respectively (Tsukui *et al.*, 2009).

The Y_1 early magma rich in plagioclase phenocrysts was ejected from the central cone. Thereafter, nearly aphyric lava effused at the base of Miharayama Central Cone. Early ejecta of the Y_1 eruption comprise orthopyroxene basalt, with 18% plagioclase and less than 0.5% orthopyroxene phenocrysts. This tephra contains approximately 17% $A1_2O_3$ and 52% SiO_2 (Fig.6). Late lava flows are aphyric basalt, containing less than 2% plagioclase and very rare orthopyroxene and augite phenocrysts. They are chemically homogeneous, containing 52.6 to 52.8% SiO_2 and approximately 14% $A1_2O_3$ (Nakano and Yamamoto, 1991).

Stop 2: Caldera-forming ejecta at Gojinkajaya (34.73945°N, 139.38144°E)

The Sashikiji 2 (S_2) Member, exposing at Gojinkajaya, was formed by an explosive eruption accompanied with caldera depression at about cal AD 340 (Yamamoto, 2006). The S_2 Member is divided into six units from S_2-a to S_2-f in ascending order (Fig. 9). The S_2-a unit consists of scoria, bomb and aa lava flows from flank fissures. The S_2-b unit is made up of well-bedded ash and fine-lapilli from the summit. The S_2-c unit is composed of matrix-supported breccia, locally filling valley bottoms and containing abundant deformed soil fragments and woods (Stop 5). The S_2-d unit consists of reverse to normal grading, clast-supported breccia with ash matrix, covering topographic relief in the whole island (Stop 2; Figs. 10 and 11). The S_2-e unit is composed of dune- to parallel-bedded lapilli and ash in the proximal facies. The S_2-f unit is clast-supported breccia with or without ash matrix. The S_2-c and -d units are quite different in sedimentological features as follows. The grain fabric measurements have revealed that the S_2-d unit has a-type imbrication showing the longest axis of grains parallel to the flow direction. On the other hand, the S_2-c has random fabric of grains. The grain size distribution of the S_2-d unit shows a bimodal nature having subpopulations at phi -1.0 to +1.0 and coarser than phi -2.5. The bimodal nature and a-type imbrication suggest that the two transport processes overlap; the load of a turbulent suspension is not all in true suspension as the coarser population may travel in a cast-dispersion mass flow. The S_2-c unit shows a polymodal grain size distribution with multi subpopulations from coarse to fine. The poor sorting, massive appearance, valley-confined distribution, and random grain fabric of the S_2-c unit are characteristic of deposition from a cohesive flow without formation of traction-related bedforms or sorting of different grain sizes by turbulence. The modal composition measurements have indicated that the S_2-c and -d units lack essential scoriaceous or glassy fragments. This evidence indicates that both units are derived from steam explosions due to outburst of highly-pressurized geothermal fluid within the edifice. The S_2-c unit was plausibly generated by remobilization of phreatic debris around the summit caused by ejection of condensed water from a plume or heavy rainfall. The S_2-d unit was a pyroclastic density current deposit resulted from collapse of a highly-discharged phreatic plume. Estimated velocities of the
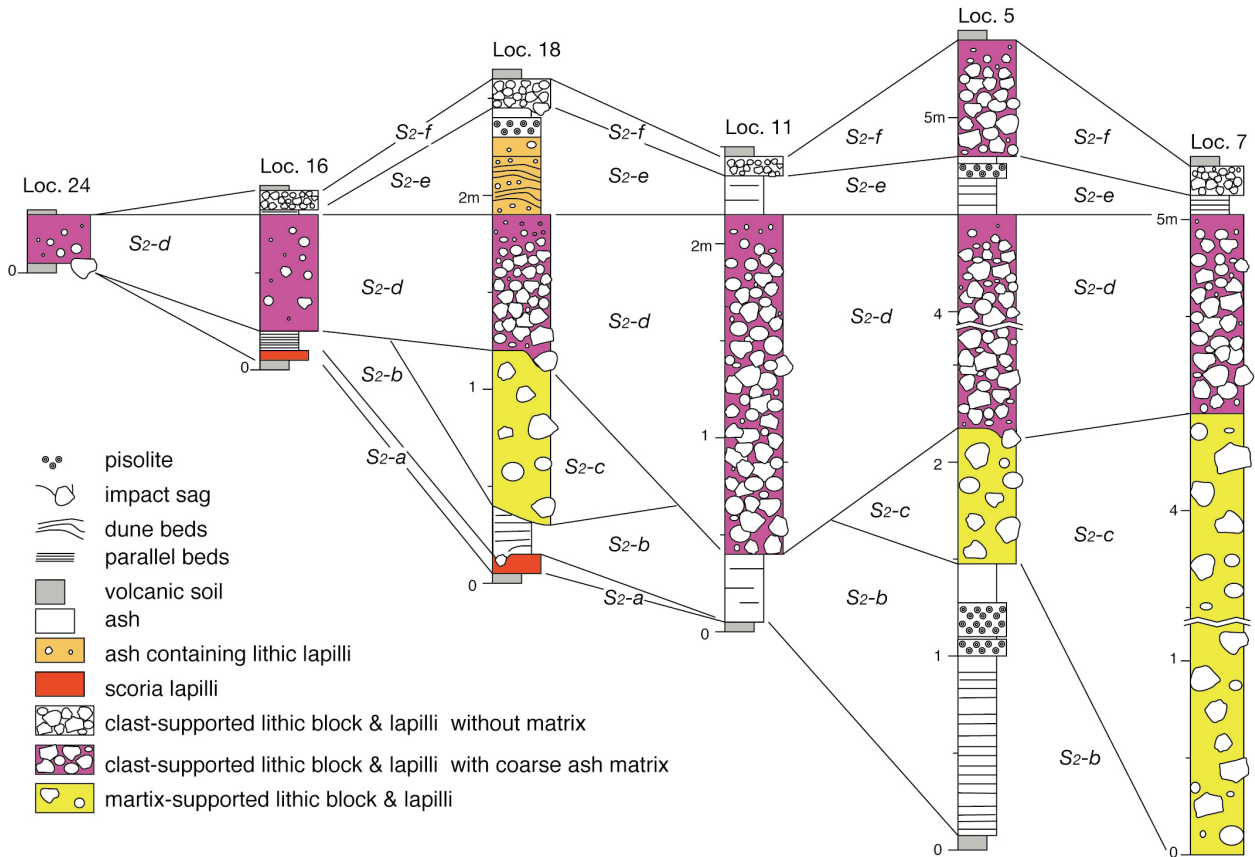
Fig. 9　Stratigraphic columns through the S_2 Member. Loc. 5 = Gojinkajaya (Stop 2). After Yamamoto (2006).

Fig.10　Reverse to normal grading, clast-supported breccia with ash matrix in the S_2-d unit (Stop 2). This breccia consists of basaltic lithic fragments without an essential material and was emplaced from a high-speed pyroclastic flow. After Yamamoto (2006).

Fig.11 Large cutting made up of abundant pyroclastic fall deposits at Chisodaisetsudanmen. Lithic pyroclastic flow deposit of the S$_2$-d unit (S2-d) pinches out toward the topographic ridge. Arrows shows impact structures at the bottom of the S$_2$-d unit.

current are 150 to 30 m/s based on suspended grain sizes.

Stop 3: Massive pile of pyroclastic fall deposits at Chisodaisetsudanmen (34.70324˚N, 139.37205E)

About 100 pyroclastic fall deposits of the younger edifice (Older Oshima Group) are exposed along road-cuttings along the southwestern coast (Fig. 11). Individual deposits are products of large-scale eruptions from the summit. Most of the deposits consist of basal scoria and overlying ash fall deposits, corresponding to the main eruption and magma-withdrawal stages. The lowest deposits of this cuttings erupted at about 20 ka. There are some unconformities within the pile of fall deposits. However, these unconformities are local and interpreted as erosion surfaces by water flushes.

The S$_2$-d lithic pyroclastic flow deposit is intercalated in the upper part of this load-cuttings (Fig. 11). Many impact sags at the base of S$_2$-d unit suggest a vigorous explosion during the caldera formation.

Stop 4: Ejecta from the Y$_4$ (1421?) fissure at the southern coast, Imasaki (34.68286˚N, 139.42441˚E)

During the Y$_4$ event, both summit and flank eruptions took place. The latter occurred along the southern part of the main rift zone (Fig. 12). The flank lava is basalt,

with less than 1% plagioclase and very rare olivine phenocrysts. The chemical compositions of the lava are quite uniform throughout, with SiO$_2$ ranging from 52.1 to 52.6% and Al$_2$O$_3$ ranging from 14.2 to 14.8% (Fig. 6). The summit lava is also basalt, and contains less than 1% plagioclase and very rare olivine phenocrysts (Nakano and Yamamoto, 1991). The chemistry is similar to that of the contemporaneous flank eruption products.

The stratigraphy of the Y$_4$ products at Imasaki shows that the flank fissures gradually expanded toward the southeast (Fig. 13). Aa lava flow from the inland Y$_4$ fissure (Y4L) are covered by partly-welded scoria rampart (Y4C) with feeder dike (Y4D), and topped by tuff breccia containing shattered glassy basalt and lithic fragments from off-shore fissures (Y4T). This Y4T unit makes elongated tuff cone with a broad crater, and generated by interactions between magma and sea water.

Stop 5: Various lahar deposits at Motomachi (34.74428˚N, 139.35563˚E)

The Izu-Oshima 2013 lahar (Fig. 14) occurred on the western steep slope of the volcano in response to heavy rain brought by the 26th Typhoon (WIPHA) on 16 October 2013. The lahar damaged Motomachi village, resulting in many fatalities. This lahar deposit consists of moderately
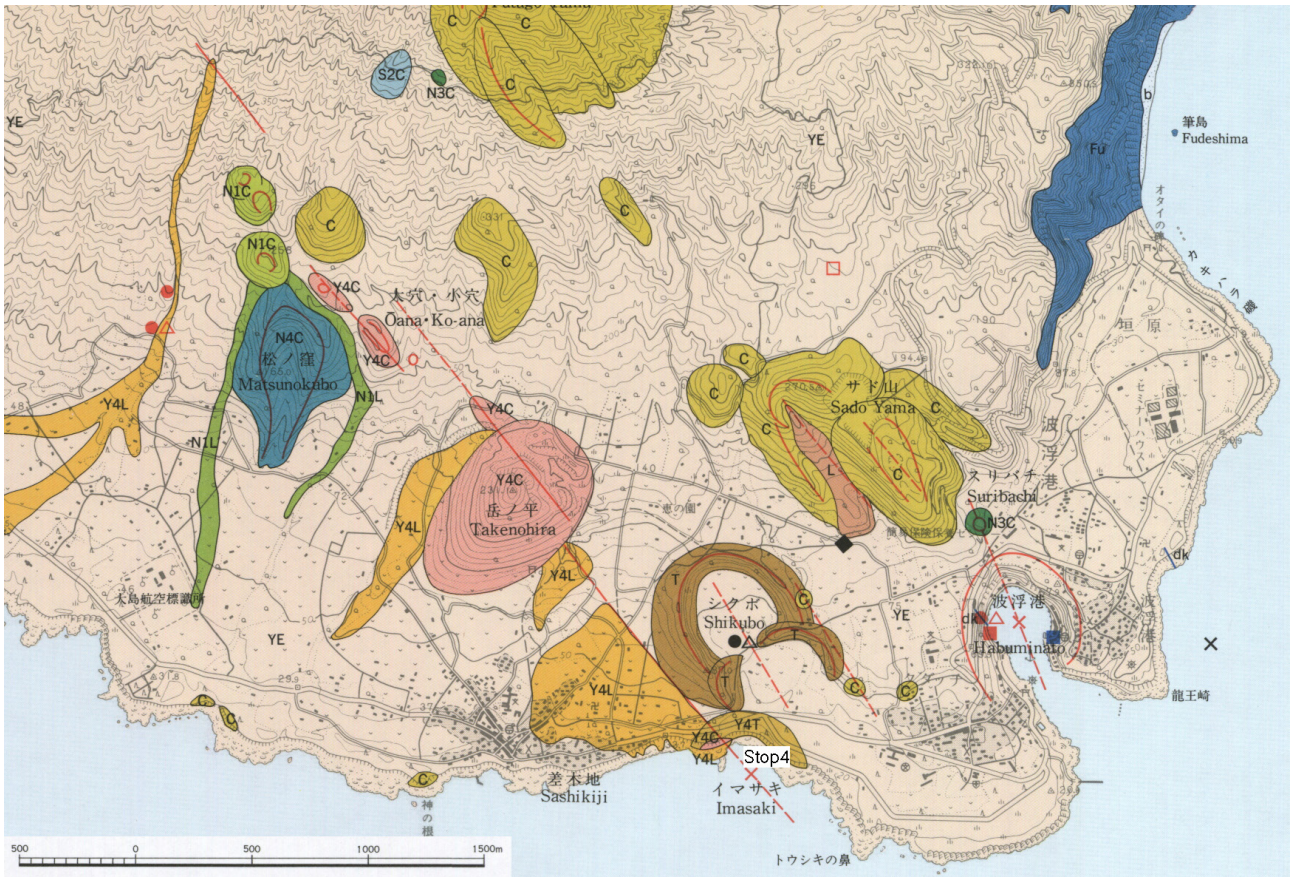
Fig. 12   Geological map of the southern part of Izu-Oshima volcano. Part of the map by Kawanabe (1998).

Fig. 13   Section of the Y_4 products from the southern fissures at Imasaki. Y4D = feeder dike of Y_4; Y4L = lava flow of Y_4; Y4C = scoria cone of Y_4; Y4T = tuff cone of Y_4; YEL = lava flow of Younger Edifice of Pre-Caldera Volcano.
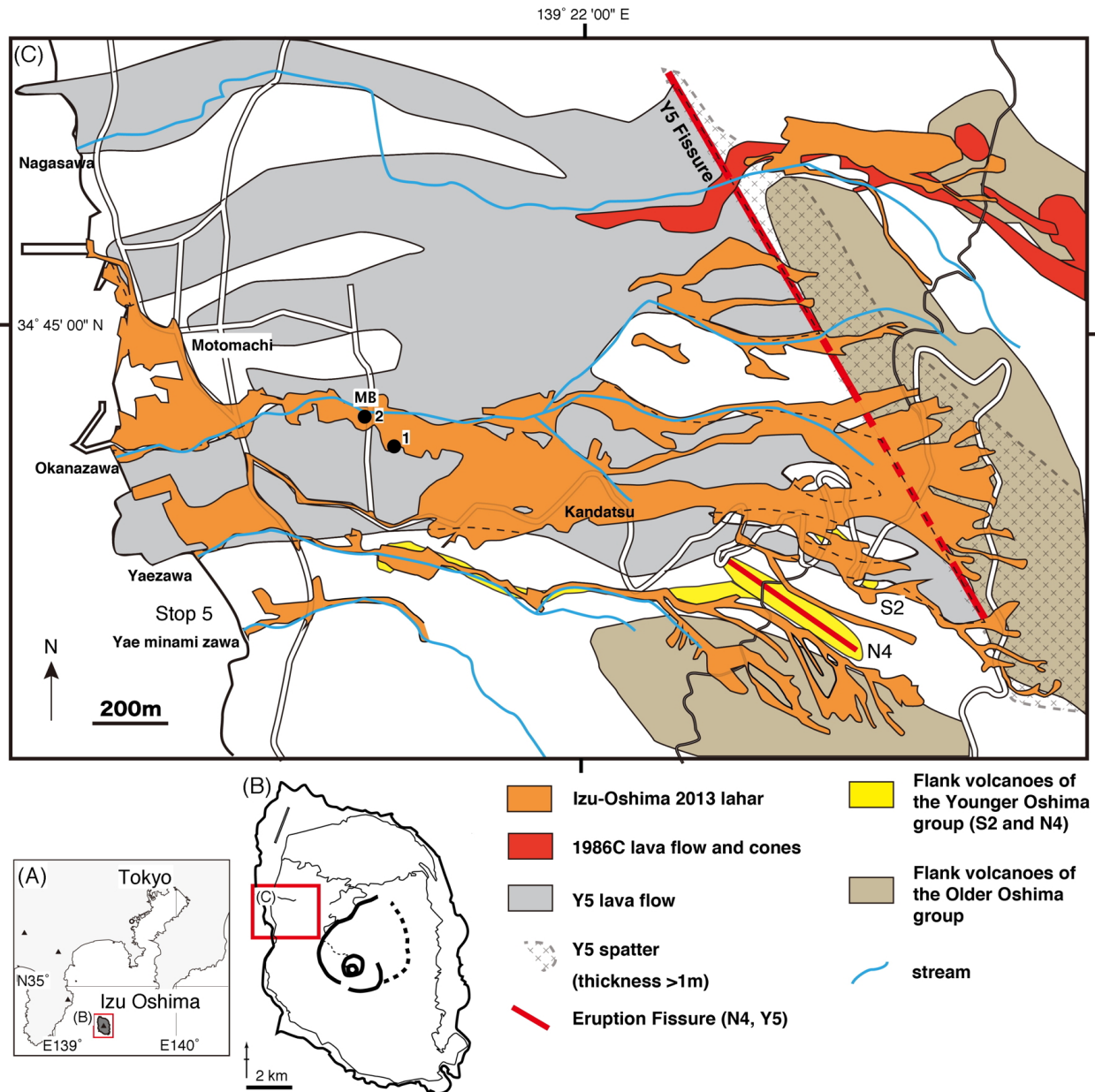
Fig. 14 Distribution of the Izu-Oshima 2013 lahar in the western part of Izu-Oshima volcano. After Yamamoto and Kawanabe (2014).

sorted, coarse- to medium-grained sand with pebbles and well-sorted fine- to very-fine-grained sand. The bi- and uni-modal grain-size distributions of the deposit suggest that the lahar was emplaced as a hyperconcentrated flood flow (Yamamoto and Kawanabe, 2014). This lahar was generated by a shallow-seated slope failure within ash fall deposits covering the Y_5-stage collapse wall, and it cascaded turbulently down to Motomachi village at high speed spreading on the slope (Fig. 15).

Hyperconcentrated flood flow deposits immediately after the Y_5 eruption and cohesive lahar deposits of the S_2-c unit are exposed along the southern coast of Motomachi (Stop 5). The earlier deposits are discontinuously bedded pebble and sand containing abundant Y_5 scoria (Fig. 16).

On the other hand, the latter deposits consist of matrix-supported gravel with wood trunks (Fig. 17).

Stop 6: Unconformity between the older edifice of Pre-caldera Izu-Oshima Volcano and Okata Volcano at Nodahama (34.79723°N, 139.36084°E)

Pre-caldera Izu-Oshima Volcano started its activity on the sea floor about 30 to 40 ka. The ejecta at this stage were mostly coarse-grained pyroclastic materials in phreatomagmatic origin. In this stop, stratified pyroclastic surge deposits during this stage abut the edifice of Okata Volcano (Fig. 18). The surge deposits contain abundant polyhedral-shaped basaltic scoria, indicating a rapid chilling effect by external water. Okata Volcano is deeply-
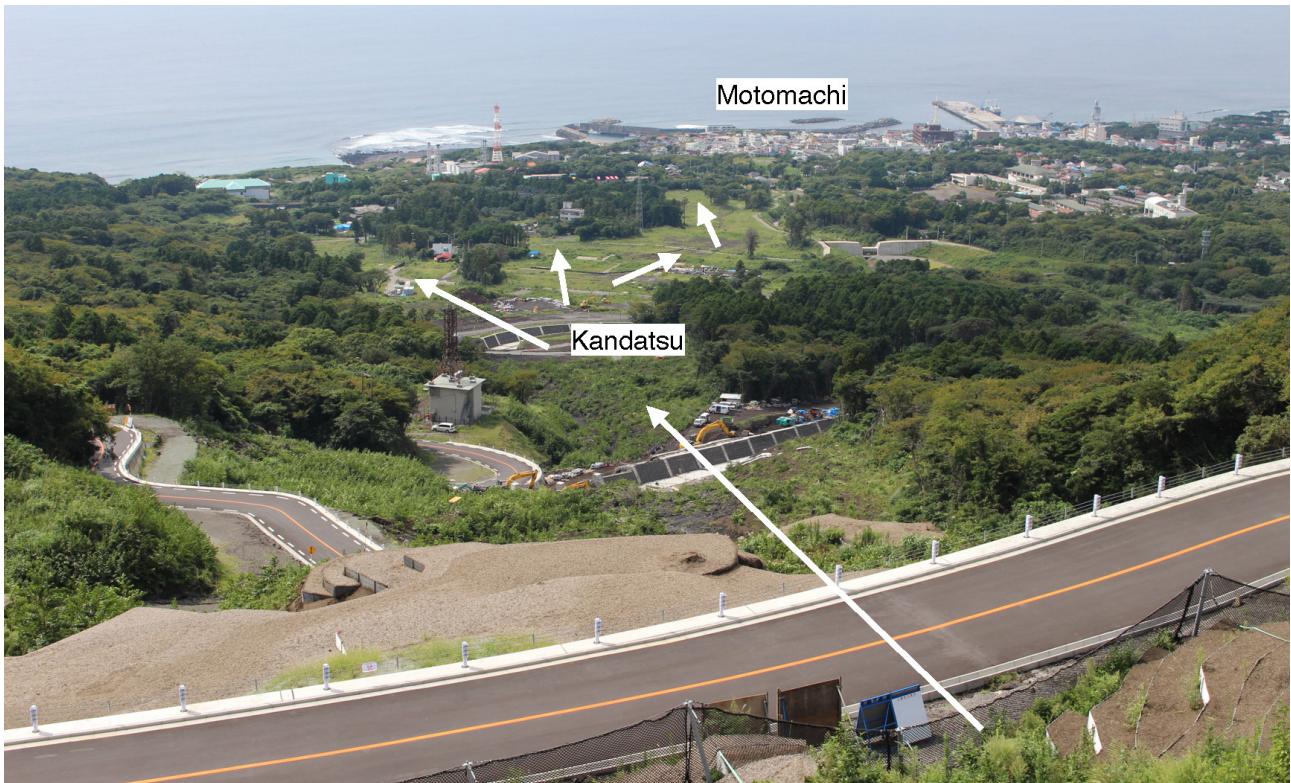
Fig. 15　Downstream path of the 2013 lahar (white arrows) from the Gojinka Sky Line. This lahar cascaded as a sheet food on this slope and destroyed houses in the Kandatsu village. Photo by 15 September, 2016.

Fig. 16　Hyperconcentrated food flow deposits of the Y_5 products at Stop 5. Lithofacies of this lahar deposite are similar to the 2013 ones and poured down the same path.

Fig. 17   Cohesive lahar deposit of the S_2-c unit (S2-c) filling a channel at Stop 5. This lahar deposit is composed of matrix-supported breccia containing deformed soli fragments and wood trunks. S1 is the ash fall deposit of the S_1 Member.

Fig. 18   Unconformity between the older edifice of Pre-caldera Izu-Oshima Volcano (OE) and Okata Volcano (Ok) at Nodahama (Stop 6).

dissected stratovolcano in the northern part of the island and composed of mainly basaltic lava flows, pyroclastic rocks, and dikes. The age of Okata Volcano is uncertain, but probably Early Pleistocene.

Acknowledgements

References

Isshiki, N.（1984） *Geology of the O Shima district*. With geological sheet map at 1 : 50,000, Geological Survey of Japan, 133p. (in Japanese with English abstract)

Kawanabe, Y.（1991） Petrological evolution of Izu Oshima volcano. *Bulletin of Volcanological Society of Japan*, **36**, 297–310. (in Japanese with English abstract)

Kawanabe, Y.（1998） *Geological map of Izu-Oshima volcano*. Geological Survey of Japan.

Kawanabe, Y.（2012） New ^{14}C ages of the Younger Oshima Group, Izu-Oshima volcano, Izu-Ogasawara arc, Japan. *Bulletin of Geological Survey of Japan*, **63**, 283–289. (in Japanese with English abstract)

Koyama, M. and Hayakawa, Y.（1996） Syn- and post-caldera eruption history of Izu Oshima volcano based on tephra and loess stratigraphy. *Journal of Geography (Chigakuzasshi)*, **105**, 133–162. (in Japanese with English abstract)

Nakamura, K.（1964） Volcano-stratigraphic study of Oshima volcano, Izu. *Bulletin of Earthquake Research Institute, University of Tokyo*, **42**, 649–728.

Nakano, S. and Yamamoto, T.（1991） Chemical variations of magmas at Izu-Oshima volcano, Japan: Plagioclase-controlled and differentiated magmas. *Bulletin of Volcanology*, **53**, 112–120.

Soya, T., Sakaguchi, K., Uto, K., Nakano, S., Hoshizumi, H., Kamata, H., Sumii, T., Kaneko, N., Yamamoto, T., Tsuchiya, N., Suto,S., Yamazaki, H., Yamaguchi, Y., Okumura, K. and Togashi, S. (1987) The l986 eruption and products of Izu-Oshima volcano.*Bulletin of Geological Survey of Japan*, **38**, 609–630.（in Japanese with English abstract）

Tsukui, M., Dangi, K., Sato, S. and Hayashi, K. (2009) Izu-Oshima volcano: precise sequence and mitigation program of the latest three large-scale eruptions revealed by historical documents. *Bulletin of Volcanological Society of Japan*, **54**, 93–112.（in Japanese with English abstract）

Yamamoto, T.（1994） Phreatomagmatic explosions: basic problems of dynamic interactions between magma and water. *Memories of Geological Society of Japan*, no.43, 63–72. (in Japanese with English abstract)

Yamamoto, T.（2006） Pyroclastic density current from the caldera-forming eruption of Izu-Oshima volcano, Japan: Restudy of the Sashikiji 2 Member based on stratigraphy, lithofacies, and eruption age. *Bulletin of Volcanological Society of Japan*, **51**, 257–271. (in Japanese with English abstract)

Yamamoto, T. and Kawanabe, Y.（2014） Sedimentary characteristics of the Izu-Oshima 2013 lahar: classification of various lahar deposits based on grain-size distribution. *Journal of Geological Society of Japan*, **120**, 233–245. (in Japanese with English abstract)

伊豆大島火山巡検ガイド

山元孝広

要　旨

　この地質ガイドは，2016年11月に開催された噴火準備過程の岩石学的解析に関する国際ワークショップの伊豆大島巡検のために作成されたものである．見学地点では，1986年噴出物，三原山火砕丘，南海岸の1421?年噴出物，1.7千年前のカルデラ形成期噴出物，先カルデラ期のテフラ層や，2013年ラハールが観察できる．

講演要旨 - Abstract

噴火準備過程の岩石学的解析に関する国際ワークショップ（PAPEMP）発表概要[*]

東宮昭彦 [1]

　噴火準備過程（マグマ蓄積や噴火トリガー等）に関する岩石学的研究は，微小領域分析手法の発展に伴って近年急速に進みつつある．こうして得られた最新の知見の共有と，関連研究者間の相互交流等を目的とし，国際ワークショップ "International Workshop on Petrological Analysis of Pre-eruptive Magma Processes (PAPEMP)"［噴火準備過程の岩石学的解析に関する国際ワークショップ］を，活断層・火山研究部門主催で行った．ワークショップは，所内 34 名・所外 42 名・合計 76 名を集め，活発な議論が行われた．以下では，国内外から招聘した 5 名の招待基調講演（30 分），および総合討論の要旨を報告する．それ以外のショートトーク（5 分）・ポスター発表については，タイトルと著者名のみを挙げる．なお，発表は全て英語で行われたが，利便性を考え，各発表の英文タイトルに和訳を付けるとともに，国内招待講演者の要旨の一部は日本語で掲載する．

Keywords: magma process, magma system, time scale, pre-eruptive magma condition, magma decompression

---

セッション 1：Deep magma processes（深部マグマプロセス）

[招待基調講演] Multiple lines of evidence for the dominance of antecrysts in arc eruptive products, and a study of crystal mushes from the Mexican Volcanic Belt（島弧噴出物がアンテクリストに富むといういくつかの証拠 – メキシコ火山帯の結晶マッシュの研究）

Georg F. Zellmer [†]

（[†] IAE, Massey University, New Zealand）

Volcanic hazard mitigation at subduction zones critically depends on knowledge of magma generation and ascent processes and timescales. Multiple lines of evidence are presented that point to crystal uptake as the principal process by which arc melts acquire their crystal cargo: (i) variable ^{234}U-^{238}U disequilibria in mineral separates; (ii) hydrous mineral rims with amorphous alteration textures; and (iii) two-pyroxene pseudo-decompression paths; cf. Zellmer *et al.* (2014a, *Geol. Soc. London Spec. Pub.*, vol. 385, p. 161–184; 2014b, *Geol. Soc. London Spec. Pub.*, vol. 385, p. 185–208) and Zellmer *et al.* (2015, *Geol. Soc. London Spec. Pub.*, vol. 410, p. 219–236). These observations point to a scarcity of true phenocrysts in arc magmas, and thus indicate rapid decompression of aphyric melts that take up their crystal cargo during ascent. The crystal cargo may thus be used to gain insights into present-day intrusive magmatic compositions and processes. For example, the Trans-Mexican Volcanic Belt (TMVB) is known for the chemical diversity in its erupted products. We have analysed the mineral chemistry of 30 geochemically well-characterized mafic eruptives from Isla Maria at the western end of the arc to Palma Sola in the east. A combination of plagioclase antecryst chemistry and MELTS thermodynamic modelling of H_2O-saturated isobaric fractional crystallization was employed to develop a pressure sensor aimed at determining the ponding depths of the co-genetic magmas from which the erupted plagioclase crystal assemblage originates. We show that the depth of magma-mush reservoirs increase eastwards along the TMVB. Magma-mush ponding depth variations fully explain the observed westward increase of average surface heat flux along the TMVB, supporting a new model of mafic arc magma ascent, where rapidly rising, initially aphyric melts pick up their antecrystic crystal cargo from a restricted crustal depth range, in which small unerupted batches of previously risen co-genetic magmas typically stall and solidify. We suggest that magma ponding is triggered by degassing-induced crystallization during magma ascent, and

---

that the pressure sensor can also be regarded as a degassing sensor, with more hydrous melts beginning to degas at greater depths. Modelled initial magma H_2O contents at the Moho range from 〜 4 to 〜 9 wt%. This implies that globally, mafic arc magmas may be used to constrain the depths of degassing and mush zone formation, as well as the amount of H_2O in the primary melts. Cf. Zellmer *et al*. (2016, *Amer. Mineral*., vol. 101, p. 2405-2422).

Keywords: antecryst, plagioclase, magma mush, ponding depth, Trans-Mexican Volcanic Belt

Snapshot of hydrous arc magma differentiation at deep crust: constraints from melt inclusion in amphibole-bearing gabbroic xenoliths（Ichinomegata maar, Northeast Japan）（東北日本・一ノ目潟マールに産する角閃石斑れい岩中のメルト包有物から制約する深部地殻領域における含水島弧マグマの分化過程）

柳田泰宏[†]

([†]東北大学)

Thermodynamic modeling of hydrous melts: Density, seismic velocity and olivine-hydrous basalt equilibrium（含水マグマの熱力学数値モデル：密度，地震波速度と，カンラン石−含水玄武岩間の平衡）

上木賢太[†]

([†]東京大学)

セッション 2：Evolution of magmatic systems（マグマ供給系の進化）

[招待基調講演] Temporal signals and magmatic histories of mushy silicic magma systems revealed by zircon chronochemistry: implications for catastrophic caldera-forming eruptions（ジルコン年代から見たマッシュ状珪長質マグマシステムの時間的シグナルとマグマ履歴および破局的カルデラ形成噴火）

Shanaka de Silva [†]

([†]CEOAS, Oregon State University, USA)

Several different pre-eruptive timescales need to be considered that characterize different stages of silicic magma system: 1) Formation of parental "mush" and associated plutonic complex ($10^5 – 10^6$ years); 2) Extraction of crystal-poor rhyolite ($10^3 – 10^2$ years); and 3) Eruption timescales that describe the transition from storage to eruption (years, months, days). Three case studies will be presented that provide valuable insight into the magmatic history and intrusive to extrusive ratios of large silicic systems.

At the 3.64 Ma Pastos Grandes caldera in SW Bolivia, Kaiser *et al*. (2017, *Earth Planet. Sci. Lett*., vol. 457, p. 73–86) show that zircon crystallized continuously for over at least 1.1 Ma while magma accumulated, erupted and eventually solidified. Such longevity is also evidenced at five Pleistocene domes in the same volcanic region. Tierney *et al*. (2016, Geology, vol. 44, p. 683–686) found essentially continuous zircon crystallization for 3.5 Ma prior to eruption. This requires time-integrated recharge rates and extremely high

intrusive to extrusive ratios of 75: 1. A similar conclusion is drawn from the U-Th in zircon systematics at Unzen volcano, Shimabara peninsula in Kyushu, Japan. Murphy *et al*. (in prep) show that while eruptive activity at Unzen is episodic over its 500 ka history, zircon crystallization was continuous, supporting the disconnect between eruptive and intrusive fluxes.

The longevity recorded in these magmatic systems supports the predictions of theoretical models that emphasize the thermomechanics of calderas (Jellinek and DePaolo, 2003, *Bull. Volcanol*., vol. 65, p. 363–381; Gregg *et al*., 2012, *Jour. Volcanol. Geotherm. Res*., vol. 241–242, p. 1–12). A thermomechanical division of calderas into smaller "brittle" systems that are triggered internally (bottom-up) while larger "ductile" systems are triggered externally (top-down) is proposed.

Keywords: pre-eruptive timescale, zircon, U-Th dating, large silicic magma reservoir, thermomechanical feedback

Relationship between temporal changes of magma-discharge rate and magmatic compositions（マグマ噴出率の時間変化とマグマ組成変化の関係）

山元孝広[†]

([†]活断層・火山研究部門)

Long-term evolution of the andesite-dacite magma system of Ruapehu volcano, New Zealand （ルアペフ火山の安山岩 - デイサイトマグマ 供給系の長期的進化）

Chris Conway [†]

([†]国立科学博物館)

Evolution of magma plumbing system of Aso volcano, SE Japan （阿蘇火山のマグマ供給系の進化）

金子克哉 [†]

([†]京都大学)

Age, petrology and chemistry of volcanic products from Omine volcano, a precursory event of Aso-4 eruption（阿蘇 -4 前駆噴火として特徴づけられる大峰火山噴出物の年代，岩石と化学組成）

長谷中利昭 [†]

([†]熊本大学)

Collapse calderas and their magma chambers （陥没カルデラとそのマグマたまり）

下司信夫 [†]

([†]活断層・火山研究部門)

セッション３：マグマプロセスのタイムスケール（Timescales of magma processes）

[招待基調講演] Timescales of magma injection and triggering processes （マグマ注入と噴火トリガー過程の時間スケール）

Fidel Costa [†]

([†]EOS, Nanyang Technological University, Singapore)

Openly degassing volcanoes are among the most active on earth (e.g., Llaima, Etna, Stromboli, Mayon, Arenal), producing mildly explosive eruptions (VEI 1–3) every few months or years. During quiescence they deliver thousands of tones of gas per day to the atmosphere. Many of these volcanoes erupt similar bulk magma composition for decades and their deposits tend to be crystal-rich. Petrological and geochemical studies show that crystals are strongly zoned (e.g. Fe/Mg in olivine and pyroxenes), which can be interpreted as evidence for shallow crystallization and partial dissolution by intrusion of a volatile-rich primitive melt in a crystal-rich shallow reservoir/conduit. However, the time scales between the first intrusion and eruption can vary significantly: at Stromboli and Etna intrusion times are days to months, whereas in Mayon or Llaima they are months and years. There seems to be a correlation between volcanoes with longer repose periods showing longer times since the first intrusions and eruption. The mass and pressure balance of open vent volcanoes suggests that magma intrusions could be induced by pressure instabilities driven by the gradual loss of mass occurring during quiescent degassing. We propose that during quiescence the shallow magma cools, degasses and crystallizes. This leads to an increase in viscosity and density of the resident magma, which becomes stiffer with time. Thus, volcanoes with longer repose times may need more magma replenishment before eruption, either through multiple intrusion episodes or larger intrusion volumes. The eruption frequencies or repose times of openly degassing volcanoes are the combined result of intrusion times (which depend on degassing fluxes) and the crystallization kinetics which depend on initial volatile contents and on heat diffusivity.

Keywords: pre-eruptive timescale, degassing, magma viscosity, repose period

Petrologic features of the magma reservoir around beginning of the Goshikidake activity, Zao volcano（蔵王火山五色岳形成開始前後の噴出物のマグマ溜まり）

西　勇樹 [†]

([†]山形大学)

Pre-eruptive process and timescale of basaltic eruption: A case study of the 2.5 ka subplinian eruption at Fuji volcano（玄武岩質噴火の噴火準備過程と時間スケール：富士山の 2.5 ka の準プリニー式噴火の例）

菅野拓矢 [†]

([†]静岡大学)

Pre-eruptive process and timescale of the 60 ka caldera-forming eruption at Hakone volcano, Japan: A preliminary results（箱根火山の 60 ka カルデラ形成噴火の噴火準備過程と時間スケール：予察的結果）

石橋秀巳[†]

([†]静岡大学)

セッション 4：Pre-eruptive conditions of magma reservoirs（噴火直前のマグマ供給系）

[招待基調講演] Pre-eruptive structure of the magma system of a caldera-forming eruption: Case studies for Shikotsu and Kutcharo volcanoes, Japan（カルデラ形成噴火前のマグマ系の構造：支笏および屈斜路火山の事例研究）

中川光弘[†]

([†]北海道大学)

　巨大噴火におけるマグマ系の形成過程と噴火過程について，複数の事例研究を積み重ね，それらの共通点と相違点を明確にすることが重要である．そのような観点から，42 ka の支笏火山と 120 ka の屈斜路火山でのカルデラ形成噴火について検討した．2 つの噴火では，主要なマグマは斑晶に乏しい(CP タイプ) 流紋岩で，それに加えて少量のデイサイト～安山岩質のマフィックマグマが認められる．支笏ではそれらに加えて，噴火活動終盤に斑晶に富む(CR タイプ) デイサイト～安山岩質マグマも共存した．鉱物組成および全岩化学組成を検討すると，CP タイプ珪長質マグマは珪長質 2 端成分マグマの混合の産物であること，また鉱物の累帯構造から，その混合は噴火の数百年前から起こっていることが明らかになった．そして 2 つの噴火では，この混合珪長質マグマに，噴火前の数年～ 10 年程度の間，マフィックマグマの貫入が噴火直前まで続いたことが明らかになった．大規模な珪長質マグマは地殻物質の部分溶融によって生じると考えられ，その場合，初期の状態では溶融で生じた結晶とメルトの混合物（マッシュ）に，地殻物質の不均質を反映した多様性が存在する可能性が高い．このことから 2 つのカルデラ噴火では，まず不均質マッシュから多様な珪長質メルトが集積・混合して大型の CP タイプメルト溜まりを形成し，そこにマフィックマグマが繰り返し貫入して巨大噴火に至ったと考えられる．このプロセスは珪長質巨大噴火で共通する可能性が高い．一方，支笏で認められる CR タイプマグマは，全岩組成や同位体比組成を考えると，CP タイプメルトが分離した残存マッシュの可能性が高い．屈斜路の場合には，CP メルトの噴出だけで噴火が終了したが，支笏の場合には最後にはマッシュの結晶主体の部分も CR タイプマグマとして噴出したと考えられる．このマグマ噴火過程の違いは，両者のカルデラ陥没深度の差に反映されていると考えられる．

Keywords: caldera-forming eruption, silicic magma, phenocryst content, magma mixing, mushy magma chamber

---

Melt inclusion constraints on pre-eruptive storage, evolution, and eruption of catastrophic caldera-forming（CCF）magma systems（メルト包有物から見たカルデラ形成マグマシステム（CCF）の噴火前マグマ蓄積・進化そして破局的噴火）

Shanaka de Silva[†]

([†]CEOAS, Oregon State University, USA)

Large caldera system and small caldera system（大カルデラシステムと小カルデラシステム）

宮城磯治[†]

([†]活断層・火山研究部門)

Conditions of the magma chamber and eruptive process of Ofunato scoria in Ofunato stage, Miyakejima volcano（三宅島火山大船戸期のマグマ溜まり条件と大船戸スコリアの噴出過程）
[ポスターのみ]

潮田雅司[†]

([†]活断層・火山研究部門)

セッション 5：Magma ascent and eruption（浅部マグマ上昇〜噴火過程）

[招待基調講演] Shallow level bifurcation of eruption styles: petrographical and experimental constraints（火道浅部での噴火様式の分岐：岩石記載と実験からの制約）

Michihiko Nakamura[†],
Mayumi Mujin[†] and Akira Miyake[‡]

([†] Graduate School of Science, Tohoku University,
[‡] Graduate School of Science, Kyoto University)

Once magmatic unrest starts, we presume a wide variety of outcomes. If we understand the mechanisms behind the branching of events, then we can utilize the results of geophysical monitoring for prediction and forecast of eruption styles effectively. A growing consensus formed in recent years is that explosive–effusive transitions often occur in shallow volcanic conduits, as evidenced by the hybrid explosive–effusive activities in which explosive and effusive eruptions occurred simultaneously (e.g. Castro *et al.*, 2014, *Earth Planet. Sci. Lett.*, vol. 405, p. 52–61). In this sense, the "pre-eruptive" period continues until the last minute before we see magmas in the Earth's surface. Such transitions in eruption style have been hardly distinguishable by using only microlite petrography. As reported by Mujin and Nakamura (2014, *Geology*, vol. 42, p. 611–614) for the 2011 Shinmoedake activity, eruption styles may be discriminated by assemblages of nanolites, i.e., groundmass minerals exhibiting a kink (break) in their CSD slopes at a few micrometers to hundreds of nanometers. The nanolite and ultrananolite are considered to have crystallized in a nearly closed, non-steady state system, because the CSD analyses in this scale are made in very small areas of dehydrated viscous melts with small turbulence within a short duration. The increase in crystal number density in a sub-micron size range should thus have been driven by accelerated increase in effective undercooling owing to extensive degassing in a shallow conduit. We additionally discovered a gap from 〜 100 to 30 nm in the size distribution of pyroxene in a dense juvenile fragment of the 2011 Vulcanian explosion, and defined the finer-sized crystals (〜30–20 nm) as "ultrananolites." Besides, Fe–Ti oxide ultrananolite ~1–2 nm in diameter was recognized with a 〜10 nm gap from titanomagnetite nanolites. These nucleation hiatuses in the late stage of groundmass crystallization are considered to have been caused by increased interfacial energy and decreased melt diffusivity in a dehydrated melt. Experimental determination of crystallization conditions of the nanolite and ultrananolite will lead to constrain bifurcation conditions of eruption styles such as minimum magma ascent rates for the sub-Plinian eruptions and maximum magma residence time in a shallow conduit for the vulcanian explosions in the Shinmoedake activity.

Keywords: explosive–effusive transition, groundmass crystallization, nanolite, ultrananolite, degassing

Evolution of magma ascent during the climactic phase of 2011 eruption of Shinmoe-dake, Japan, in view of groundmass microlite textures（石基マイクロライト組織から見た 2011 年新燃岳噴火最盛期におけるマグマ上昇過程の進化）

鈴木由希[†]

([†] 早稲田大学)

On progress and rate of the peritectic reaction of olivine to pyroxene, with implications for the growth rates of microlites at the onset of eruption（かんらん石 - 輝石の包晶反応の進行と速度：噴火開始時のマイクロライト成長速度への影響）

Georg F. Zellmer[†]

([†] IAE, Massey University, New Zealand)

Magma ascent process of the 2000 eruption at Miyakejima volcano deduced from melt inclusion analyses（メルト包有物からみた三宅島火山 2000 年噴火のマグマ上昇過程）

斎藤元治[†]

([†] 活断層・火山研究部門)

Temporal change in microstructure of volcanic ashes from Aso Nakadake 2014–2015 eruption（阿蘇中岳 2014–2015 年噴火で噴出した火山灰の微細組織の時間変化）[ポスターのみ]

大槻静香[†]

([†] 活断層・火山研究部門)

General discussions（総合討論）

Summary of the general discussions （総合討論の概要）

Shanaka de Silva [†] （moderator）

（[†] CEOAS, Oregon State University, USA）

1) Deep magma processes — what do we think we know?
- Crystal cargo from deep offers an opportunity to probe plutonic system (Zellmer)
- Crystal extract is within melt of much more evolved composition (Yanagida)
- Water content of melts controls seismic velocities (Ueki)

2) Evolution of magma systems　— what do we think we know?
- Variable time scales for different parts of the system (de Silva)
- Variable eruptive fluxes at different volcanoes (Yamamoto)
- Progressive magma fluxes can erode fertility (Conway)
- Deep melting can produce silicic magmas (Kaneko)
- Omine volcano might be a precursor and trigger to Aso 4 (Hasenaka)
- Mixing and unmixing of magmas during Aira caldera evolution (Geshi)

3) Timescales — what do we think we know?
- Different time scales for different stages of the system (de Silva)
- Cause and effect? — temporal relationships don't always mean a causations (Costa)
- Need to look at processes leading to eruption rather than focus on a trigger (Costa)
- Degrees of mixed magma development control eruptive style (Nishi)

4) Pre-eruptive magma conditions — what do we think we know?

- Recharge, hybridization and depth of extraction explains the difference between Shikotsu and Kutcharo (Nakagawa)
- Melt inclusion data - shallow storage and evolution of CCF magma systems; may control eruptive transition from explosive to effusive (Grocke/de Silva)
- Petrological forensics using experimental and MELTS approach allows geophysical parameters of magma chambers to be developed (Miyagi)

5) Magma Ascent and Eruption — what do we think we know?
- Discovery of nanolites and ultrananolites requires us to think about what CSD's are telling us about conduit processes — volcanic glass may not be glass (Nakamura)
- Decompression experiments are critical to resolving this (Nakamura)
- Same magma may follow divergent decompression paths (Suzuki)

6) What do we know that we don't know?
- What controls the variable histories of similar volcanoes?
- Time scales
  - Arrhenius relationship: Diffusion coefficients, Temperature
  - Nature of recharge — continuous vs step-wise recharge
- What do we mean by "trigger"?
  - What are the triggers?
  - How do we know what is important? Recharge as a universal trigger?
- CSD's, nucleation/growth
  - Decompression rate recorded in microlites
  - Where divergence of decompression occurs

地質調査総合センター研究資料集

地質調査総合センターの最新出版物

---

5 万分の 1 地質図幅	母島列島・新潟及び内野・播州赤穂・観音寺	
20 万分の 1 地質図幅	横須賀（第 2 版）・大分（第 2 版）・松山（第 2 版）	
200 万分の 1 地質編集図	No. 4	日本地質図（第 5 版）
	No. 11	日本の火山（第 3 版）
特殊地質図	No. 12	富士火山地質図（第 2 版）
	No. 33	日本周辺海域鉱物資源分布図（第 2 版）
海洋地質図	No. 87	金華山沖表層堆積図（1:20 万）
	No. 88	見島沖海底地質図（1:20 万）
火山地質図	No. 18	蔵王火山地質図（1:2.5 万）
	No. 19	九重火山地質図（1:2.5 万）
水文環境図	No. 9	富士山
空中磁気図	No. 46	養老断層地域高分解能空中磁気異常図
	No. 47	富士火山地域高分解能空中磁気異常図
重力図	No. 32	和歌山地域重力図（ブーゲー異常）
	S3	甲府地域重力構造図（ブーゲー異常）
構造図	No. 14	全国主要活断層活動確率地図
海外地球科学図	アジア鉱物資源図（1:500 万）	
	東アジア地域地震火山災害情報図（1:1000 万）	
海陸シームレス地質図	S-5	海陸シームレス地質情報集「駿河湾北部沿岸域」
燃料資源図	FR-3	燃料資源地質図「関東地方」
土壌評価図	E-7	表層土壌評価基本図「高知県地域」
数値地質図	G-16	20 万分の 1 日本シームレス地質図　DVD 版
	G-17	九州地質ガイド
	GT-4	全国地熱ポテンシャルマップ
	V-3	口永良部島火山地質データベース
	P-2	日本重力データベース　DVD 版
	G20-1	20 万分の 1 数値地質図幅集「北海道北部」第 2 版
	G20-2	20 万分の 1 数値地質図幅集「北海道南部」第 2 版
その他	日本の熱水系アトラス	
	海と陸の地球化学図	
	関東の地球化学図	

BULLETIN
OF THE
GEOLOGICAL SURVEY OF JAPAN

Vol. 68　No. 4　2017

CONTENTS